Journal Pre-proof

Incorporation of SARS-CoV-2 spike NTD to RBD Protein Vaccine Improves Immunity Against Viral Variants

Isabelle Montgomerie, Thomas W. Bird, Olga R. Palmer, Ngarangi C. Mason, Theresa E. Pankhurst, Blair Lawley, Leonor C. Hernández, Rhodri Harfoot, Astrid Authier-Hall, Danielle E. Anderson, Kerry L. Hilligan, Kaitlin H. Buick, Naasson M. Mbenza, Gerd Mittelstädt, Samara Maxwell, Shubhra Sinha, Joanna Kuang, Kanta Subbarao, Emily J. Parker, Alan Sher, Ian F. Hermans, James E. Ussher, Miguel E. Quiñones-Mateu, Davide Comoletti, Lisa M. Connor, On behalf theVAANZ Group

PII: S2589-0042(23)00333-4

DOI: https://doi.org/10.1016/j.isci.2023.106256

Reference: ISCI 106256

To appear in: *ISCIENCE*

Received Date: 28 September 2022

Revised Date: 10 January 2023

Accepted Date: 17 February 2023

Please cite this article as: Montgomerie, I., Bird, T.W., Palmer, O.R., Mason, N.C., Pankhurst, T.E., Lawley, B., Hernández, L.C., Harfoot, R., Authier-Hall, A., Anderson, D.E., Hilligan, K.L., Buick, K.H., Mbenza, N.M., Mittelstädt, G., Maxwell, S., Sinha, S., Kuang, J., Subbarao, K., Parker, E.J., Sher, A., Hermans, I.F., Ussher, J.E., Quiñones-Mateu, M.E., Comoletti, D., Connor, L.M., On behalf theVAANZ Group, Incorporation of SARS-CoV-2 spike NTD to RBD Protein Vaccine Improves Immunity Against Viral Variants, *ISCIENCE* (2023), doi: https://doi.org/10.1016/j.isci.2023.106256.

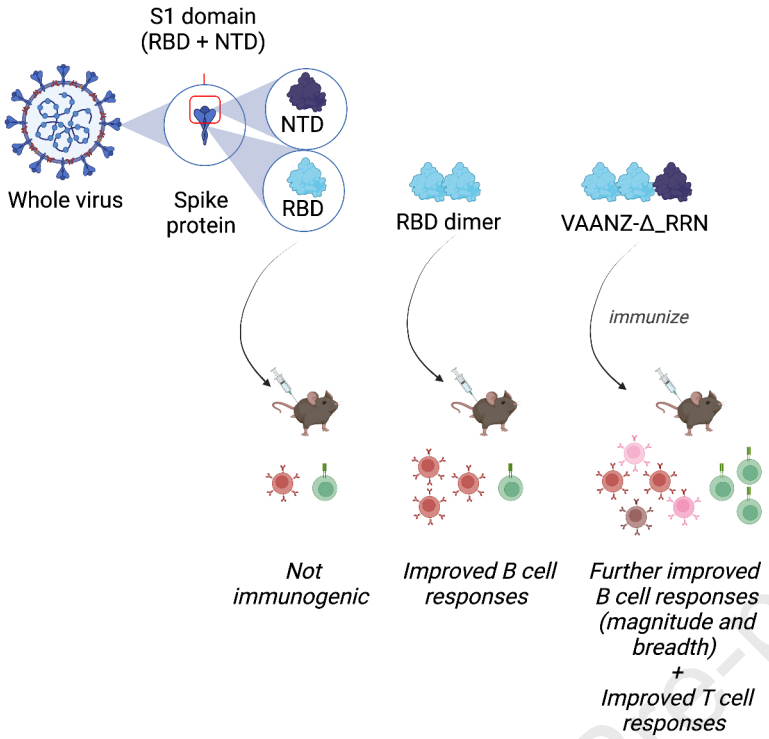

Incorporation of SARS-CoV-2 spike NTD to RBD Protein Vaccine Improves Immunity Against Viral Variants

Authors: Isabelle Montgomerie [1], Thomas W. Bird [1], Olga R. Palmer [2], Ngarangi C. Mason [2], Theresa E. Pankhurst [2], Blair Lawley [3], Leonor C. Hernández [3], Rhodri Harfoot [3], Astrid Authier-Hall [2], Danielle E. Anderson [4], Kerry L. Hilligan [2,5], Kaitlin H. Buick [2], Naasson M. Mbenza [1], Gerd Mittelstädt [6], Samara Maxwell [1], Shubhra Sinha [3], Joanna Kuang [3], Kanta Subbarao [4,7], Emily J. Parker [6], Alan Sher [5], Ian F. Hermans [2], James E. Ussher [3], Miguel E. Quiñones-Mateu [3,8 *], Davide Comoletti [1*], Lisa M. Connor [1, 2,*], On behalf the VAANZ Group

Affiliations: *[1]Victoria University of Wellington, Wellington, New Zealand; School of Biological Sciences.*

[2] Malaghan Institute of Medical Research, Wellington, New Zealand.

[3]Department of Microbiology and Immunology, School of Biomedical Sciences, University of Otago, Dunedin, New Zealand.

[4] Department of Microbiology and Immunology, University of Melbourne, at The Peter Doherty Institute for Infection and Immunity, Melbourne, Victoria.

[5]Laboratory of Parasitic Diseases, National Institutes of Health, Bethesda, USA.

[6]Victoria University of Wellington, Wellington, New Zealand; Ferrier Institute of Research.

[7]WHO Collaborating Centre for Reference and Research on Influenza

[8]Webster Centre for Infectious Diseases, University of Otago, Dunedin, New Zealand.

* Corresponding Authors and Request for Reprints: M.E.Q-M, Department of Microbiology and Immunology, University of Otago, Dunedin, New Zealand, Phone: +64 3 479 7703, E-mail: miguel.quinones-mateu@otago.ac.nz; D.C., Victoria University of Wellington, Wellington, New Zealand, Phone: +64 4 463 6029, Email: davide.comoletti@vuw.ac.nz; L.M.C., Victoria

University of Wellington, Wellington, New Zealand, +64 4 463 5339, Email: lisa.connor@vuw.ac.nz

Lead contact: L.M.C., Victoria University of Wellington, Wellington, New Zealand, +64 4 463 5339, Email: lisa.connor@vuw.ac.nz

Summary: Emerging SARS-CoV-2 variants pose a threat to human health worldwide. SARS-CoV-2 receptor binding domain (RBD)-based vaccines are suitable candidates for booster vaccines, eliciting a focused antibody response enriched for virus neutralizing activity. Although RBD proteins are manufactured easily, and have excellent stability and safety properties, they are poorly immunogenic compared to the full-length spike protein. We have overcome this limitation by engineering a subunit vaccine composed of an RBD tandem dimer fused to the N-terminal domain (NTD) of the spike protein. We found that inclusion of the NTD (i) improved the magnitude and breadth of the T cell and anti-RBD response, and (ii) enhanced T follicular helper cell and memory B cell generation, antibody potency, and cross-reactive neutralization activity against multiple SARS-CoV-2 variants, including B.1.1.529 (Omicron BA.1). In summary, our uniquely engineered RBD-NTD-subunit protein vaccine provides a promising booster vaccination strategy capable of protecting against known SARS-CoV-2 variants of concern.

Key words: SARS-CoV-2, COVID-19, vaccine, receptor binding domain, N terminal domain

Abbreviations: SARS-CoV-2, Severe acute respiratory syndrome coronavirus 2**;** RBD, Receptor binding domain; NTD, N terminal domain**;** ACE2, Angiotensin converting enzyme 2; NAbs, neutralizing antibodies; GC, germinal center; AP, alkaline phosphatase; iLN, inguinal lymph nodes.

INTRODUCTION

COVID-19, the disease caused by severe acute respiratory syndrome coronavirus 2 (SARS-CoV-2), has had a profound impact on human health at a global scale and is responsible for the deaths of more than 6 million people. The first generation of COVID-19 vaccines have been highly successful in controlling the disease and minimizing death[1,2], but as the virus continues to evolve, alternative vaccine approaches may be more appropriate for boosting existing immunity.

SARS-CoV-2 mediates cell entry through the viral spike protein binding to its receptor protein, angiotensin converting enzyme 2 (ACE2) on host epithelial cells[3-5]. As such, the spike protein has been the target for most vaccine strategies[6,7]. The SARS-CoV-2 spike is a homotrimer, where each monomer is composed of an S1 and S2 domain[4]. The S1 domain consists of an N terminal domain (NTD) followed by the receptor binding domain (RBD), which directly interacts with ACE2. The S2 domain mediates viral membrane fusion[7]. Antibody mediated protection against SARS-CoV-2 is almost entirely mediated by anti-RBD antibodies, followed by anti-NTD antibodies[8-15]. While S2 domain antibodies can disrupt viral membrane fusion, these represent a much smaller proportion of neutralizing antibodies (NAbs)[16-20]. Non-neutralizing S2 domain targeting antibodies are common in naïve and post infection individuals[19].

Emerging evidence suggests that neutralizing antibody titers wane after two COVID-19 vaccine doses[21] and immunity against highly mutated Omicron variants is significantly reduced after three months post boost (third administration)[22]. Thus, booster vaccination strategies are

required to control the pandemic. New vaccine designs should focus the humoral response on the RBD to drive high levels of NAbs and avoid the risk of repriming immune responses towards non-neutralizing epitopes. However, the RBD alone is a poor immunogen, generally failing to generate high levels of NAbs[23,24]. In a whole spike immunization or in an infection, the body encounters the RBD within a homotrimer, and the NTD and S2 domains provide additional T cell epitopes. The poor immunogenicity of the RBD can be improved by multimerization, allowing for improved B cell receptor crosslinking[25] and more efficient phagocytosis by antigen presenting cells [26]. Immunization with a tandem dimer of the RBD generates high levels of NAbs [27], and protects mice from infection following live SARS-CoV-2 challenge[28]. However, dimerization does not compensate for the minimal $CD4^+$ T cell epitopes in the RBD, which play an important role in driving cross-reactive immunity against emerging variants by encouraging germinal center reactions[29,30]. The S1 domain has been shown to be a more effective immunogen in animal models than the RBD monomer[24]. This is likely due to the additional epitopes contained within the NTD of S1, that elicit both CD4 T cell responses[31,32] and NAbs[11,12].

In this study, we introduce a subunit vaccine strategy designed to enrich for RBD-specific antibodies and prevent the accumulation of non-neutralizing S2 domain targeting antibodies. Our novel protein subunit vaccine contains a tandem-dimer RBD with the NTD fused at the C terminus (RBD-RBD-NTD), combining high protein expression with the presence of both NTD and RBD epitopes. Unlike vaccines based on the entire spike protein, our innovative strategy excludes the S2 domain, reducing the risk of magnifying pre-existing non-neutralizing S2 domain antibodies [33]. Mice immunized with our RBD-RBD-NTD subunit vaccine (referred to hereafter as VAANZ-Δ_RRN) showed equivalent protection to that seen in SARS-CoV-2 convalescent mice.

Incorporation of the NTD resulted in an increased T cell response and improved affinity and breadth of the antibodies generated, ultimately conferring greater cross-neutralizing capacity compared to an RBD tandem dimer vaccine. By focusing the host humoral response to the receptor binding and N terminal domains of the SARS-CoV-2 spike protein, we show that VAANZ-Δ_RRN can be a suitable candidate for a booster vaccine against circulating, and perhaps novel, SARS-CoV-2 variants.

RESULTS

Development of subunit vaccine candidate. We sought to increase immunogenicity and T cell response to an RBD-protein based vaccine by dimerizing the RBD and adding the NTD to the RBD-dimer construct. Our vaccine design was based on evidence that tandem dimerization of the RBD promotes a significant increase in the expression of the recombinant protein and improves immunogenicity in mice [28]. In addition, mapping of the distribution of $CD4^+$ and $CD8^+$ T cell epitopes in COVID-19 cases revealed that the NTD was particularly immunodominant [32]. Based on these findings, we engineered a series of constructs with a tandem RBD sequence and one copy of the NTD. The first series of constructs were based on ancestral (Wuhan, W) sequences, followed by a second generation of constructs based on the SARS-CoV-2 Delta variant (Figs. 1A-C). The monomeric RBD construct (W_RBD) and the RBD tandem dimer (W_RBD-RBD) included residues 329-537 of the ancestral sequence (Figs. 1A and 1B). To evaluate impact of design architecture on expression, stability, and binding of ACE2, controls consisting of an RBD monomer, an RBD tandem dimer from each strain, and an RBD-NTD heterodimer were also prepared, as shown in cartoons in Figure 1C. For the constructs containing the NTD, optimization of the interdomain linkers and the RBD-NTD arrangement was required to improve expression.

We found that transposing the NTD to the RBD C-terminus improved expression. Thus, our initial protein candidate was developed using the RBD-RBD-NTD architecture, hereafter referred to as VAANZ-W_RRN. (Fig. 1C).

To increase expression and to streamline protein production, cell lines were made for all constructs used in this study, as detailed elsewhere [34]. The expression level of the different constructs varied between ~5 and 30 mg/L of media after purification. The proteins were routinely purified to at least 90% purity, as verified by size-exclusion chromatography (SEC) and SDS-PAGE followed by Coomassie stain (Supp. Fig. 1A-D). Thermostability assays (TSA) were also used to assess the folding and stability of the purified proteins over several months at 4°C. Importantly, all proteins maintained the same TSA parameters for at least 5 months at 4°C (Supp. Fig. 1E), indicating the RBD-based proteins are very stable at this temperature. These proteins maintained the three-dimensional structure of the SARS-CoV-2 RBD, as evidenced by the ACE2 binding (Supp. Fig. 1F). The ACE2 binding affinity was assessed for the W_RBD, W_RBD-RBD and VAANZ-W_RRN proteins. Affinity calculations revealed that dimerizing the RBD doubled the binding affinity to ACE2 (W_RBD = Kd of 3.82 nM W_RBD-RBD = Kd of 1.87 nM). Furthermore, the Kd of all other constructs tested here was very similar at <2 nM, suggesting that the inclusion of the NTD domain in VAANZ-W_RRN protein did not impact ACE2 interaction (Supp. Fig. 1F). In summary, all constructs were correctly folded and the inclusion of the NTD at the C terminus of the RBD dimer did not impact the RBD/ACE2 interaction, and as such all domains are still available for antibody targeting.

In order to address the emergence of the highly transmissible SARS-CoV-2 Delta variant in December 2020[35], we developed a new RBD-RBD-NTD construct based on this variant, termed

VAANZ-Δ_RRN (Fig. 1A). Notably, the expression level of the SARS-CoV-2 Delta variant version increased approximately 6-fold compared to the ancestral strain construct and displayed similar ACE2 binding properties (VAANZ-W_RRN = Kd of 1.72 nM, VAANZ-Δ_RRN = Kd of 1.81 nM).

Immunization with VAANZ-W_RRN and VAANZ-Δ_RRN **provide protection equivalent to that seen in convalescent mice.** To determine whether VAANZ-Δ_RRN, containing the critical epitopes of the S1 domain, was sufficient to confer protection, we tested its protective capacity in an animal model. K-18 mice carry the human ACE2 protein on the keratin 18 promoter, and therefore express ACE2 on epithelial cells, including the respiratory mucosa, which make them highly susceptible to infection with SARS-CoV-2 [36-38]. Mice were unvaccinated or immunized on day 0 and 21 with 50 μg of VAANZ-Δ_RRN AddaVax™. Given the strong protective capacity of previous SARS-CoV-2 infection for subsequent infection [39], as a positive control to benchmark the efficacy of our novel subunit vaccine, a convalescent group of mice was established using a sub-lethal dose inoculation of 10^2 $TCID_{50}$ SARS-CoV-2 (SARS-CoV-2/Australia/Vic/01/20 (ancestral; Wuhan-1 like SARS-CoV-2 (Wuhan)) on day 14. On day 35, all groups of mice were intranasally challenged with 1 x 10^4 $TCID_{50}$ of SARS-CoV-2 (SARS-CoV-2/Australia/Vic/18440/2021 (B.1.617.2, delta variant)) and then monitored for body weight changes and mortality (Fig 2A). Infection of unvaccinated mice resulted in rapid weight loss, and by day 16 61.5% of mice had succumbed to SARS-CoV-2 infection (Fig 2B-C). However, all mice immunized with VAANZ-Δ_RRN + AddaVax™ were protected from SARS-CoV-2 disease and did not lose any body weight (Fig. 2C). Viral titers in the lung and nasal turbinates of SARS-CoV-2 challenged mice were similar in immunized and convalescent groups (Fig 2D). In the case of

immunization with VAANZ-W_RRN, and challenge with ancestral SARS-CoV-2 a similar level of protection from weight loss was observed (Supp. Fig. 2A-B) and 100% of mice survived, as opposed to 7% in the unvaccinated group.

Next, we investigated whether protection conferred from immunization with VAANZ-W_RRN correlated with the presence of NAbs. C57BL/6 mice were immunized twice with PBS, or 50 μg VAANZ-W_RRN + AddaVax™, on days 0 and 21, and serum was collected at day 28. We compared the neutralization capacity of sera samples from immunized mice with that of convalescent human sera against SARS-CoV-2 (NZ/Queenstown/01 strain) in a replication-competent virus neutralization assay. Mice immunized with VAANZ-W_RRN showed a 2.5-fold higher neutralizing antibody titer compared to serum samples from convalescent humans (Supp. Fig 2D).

To assess the durability of the antibody response initiated by VAANZ-W_RRN and VAANZ-Δ_RRN we tracked anti-RBD IgG titers over time compared to titers in mice immunized with formalin-inactivated SARS-CoV-2 (resembling approved COVID-19 vaccines currently administered to millions worldwide[40,41]). Similar to the formalin-inactivated virus, antibody levels in VAANZ-W_RRN vaccinated mice peaked at approximately 70 days after the first dose and then plateaued 100 days after the second dose, remaining stable for at least 220 days (Supp. Fig 2E). Likewise, anti-RBD IgG in VAANZ-Δ_RRN vaccinated mice persisted for 384 days (Fig 2E). These data suggest that, despite the smaller size of the dimerized RBD and NTD protein, compared to full length spike protein, protection and neutralizing antibody was comparable to responses elicited by the whole virus.

The T cell response induced by ancestral- and Delta-based constructs were also similar. Groups of C57BL/6 mice were immunized on day 0 and 21 with 50 μg of VAANZ-W_RRN or VAANZ-Δ_RRN with AddaVax™ or were treated with PBS as a negative control. To assess the T cell response, on day 28 IFN-γ ELISpot assays were performed on splenocytes restimulated with overlapping peptide pools from the S1 domain of the respective variants. Immunization with either ancestral- or Delta-based RBD-RBD-NTD protein induced similar number of IFN-γ-producing T cells specific for S1 (Fig. Supp 2F). Likewise, both protein constructs induced similar titers of RBD binding antibodies (Fig. Supp 2G). Given that (i) the production yield of VAANZ-Δ_RRN was 6X greater than the ancestral construct (ii) there was no difference in the immunogenic profile or protective capacity between the two constructs we decided to develop VAANZ-Δ_RRN as our primary vaccine candidate.

Incorporation of the NTD enhances immunogenicity of the RBD subunit vaccine.

To determine whether the addition of the NTD within VAANZ-Δ_RRN resulted in an increased breadth of T cell response, we compared the antigen-specific response to vaccination with a Delta variant RBD dimer (Δ_RBD-RBD). T cell responses against the different regions of spike protein were assessed by restimulation with overlapping peptide pools from RBD or S1 (RBD + NTD). When mice were immunized with Δ_RBD-RBD, there was no significant difference between the number of RBD-specific or S1-specific IFN-γ-producing T cells. In contrast, immunization with VAANZ-Δ_RRN resulted in significantly higher numbers of S1-specific IFN-γ-producing T cells than RBD-specific cells (Fig. 3A), a difference most likely due

to a T cell response against the NTD. To assess the contribution of NTD-specific T cells to the total IFN-γ-producing response, we measured the ratio of S1 to RBD specific IFN-γ-producing T cells, showing that for every RBD-specific IFN-γ^+ cell, there were, on average, two S1-specific cells when mice were immunized with VAANZ-Δ_RRN. Therefore, addition of the NTD to the RBD dimer significantly improved the T cell response by providing additional T cell epitopes (Fig. 3B).

Given that vaccination with VAANZ-Δ_RRN promoted enhanced T cell immunity compared to the RBD dimer, we investigated whether a higher number and frequency of T follicular helper (T_{FH}) cells were induced, as these cells are critical for B cell activation, class switching and affinity maturation [42]. Expression levels of the T_{FH}-associated molecules B-cell lymphoma 6 protein (Bcl6) and programmed death-1 (PD-1) on $CD4^+$ T cells from the draining lymph node (LN) (Fig. 3C) revealed that indeed, the incorporation of the NTD promoted a higher number and proportion of T_{FH} cells (Figs. 3D and 3E).

Next, we determined whether the inclusion of the NTD in the VAANZ-Δ_RRN protein improved the antibody response to RBD. Immunization with VAANZ-Δ_RRN induced higher levels of anti-RBD IgG antibodies (Fig. 3H) compared to titers in mice immunized with the Δ_RBD-RBD protein. To gain a more detailed understanding of the humoral response induced following immunization with the different RBD protein vaccines, we evaluated the antigen-specific B cell responses in vaccinated mice by flow cytometry. To detect antigen-specific B cells we made fluorescent tetramers of the S1 domain (Wuhan, Delta, Kappa, Beta, and omicron S1 tetramers all on PE), which includes epitopes present in VAANZ-Δ_RRN protein. A control

tetramer of ovalbumin (OVA) was also generated to detect cells binding non-specifically. Draining lymph nodes were isolated 7 days after the second immunization with VAANZ-Δ_RRN or Δ_RBD-RBD and labelled with B cell tetramers and mAbs for cell surface markers identifying plasma cells ($CD19^{+}$, $B220^{-}$, $IgD^{-,}$ $IRF4^{high}$, $CD138^{high}$), memory cells ($B220^{+}$, IgD^{-}, $CD38^{high}$, $GL7^{low}$) and germinal center (GC) cells ($B220^{+}$, $IgD^{-,}$ $CD38^{low}$, $CD95^{+}$ $GL7^{high}$, $BCL6^{+}$) (Supp. Fig. 5). S1-specific B cells were only detected in immunized mice, and higher numbers were detected in VAANZ-Δ_RRN vaccinated mice compared to the Δ_RBD-RBD group (Figs. 3G-J). Overall, the enhanced S1-specific responses observed after VAANZ-Δ_RRN immunization compared to Δ_RBD-RBD immunization were the result of preferential expansion of memory B cells (Fig. 3J). Importantly, an enhanced frequency of B cells expressing a memory phenotype is a good indication of vaccine durability and is therefore particularly encouraging for this vaccine candidate. Together these data support our original vaccine design rationale, whereby fusing the NTD onto the RBD-RBD protein enhances T cell immunity, which in turn supports B cell immunity and overall, improves immunogenicity of the protein antigen [39].

VAANZ-Δ_RRN provides cross protection against SARS-CoV-2 variants of concern. A successful booster vaccine should provide protective cross-reactive antibodies that can confer protection against multiple variants of concern as well as potentially novel variants. To assess the cross-reactivity of VAANZ-Δ_RRN, we generated a panel of pseudotyped lentiviruses expressing the spike glycoprotein from a number of SARS-CoV-2 variants of concern, i.e., from B.1.1.7 (Alpha) to B.1.1.529 (Omicron BA.1), as well as SARS-CoV [43]. Similar to previous studies [44], we first validated this comprehensive panel by comparing the neutralization activity of serum samples from immunized mice or convalescent COVID-19 individuals, as well as an anti-spike mAb and

soluble ACE2 protein, showing equivalent neutralization titers using authentic SARS-CoV-2 and SARS-CoV-2 spike pseudotyped viruses (Supp. Fig. 4). Next, given that the broadly used Pfizer-BioNTech mRNA vaccine (BNT162b2) provides 95% protection against ancestral SARS-CoV-2 infection [45], here we used serum samples from individuals vaccinated with BNT162b2 to determine NAb titers against the ancestral SARS-CoV-2 spike. Another relevant comparative benchmark is the NAb levels that correlate with protection in mice. K18-ACE2 transgenic mice vaccinated with VAANZ-W_RRN were completely protected from live SARS-CoV-2 intranasal challenge (Supp. Figs. 2B and 2C). We used these neutralization titers to benchmark NAb responses obtained with VAANZ-Δ_RRN in mice as an indicator of the NAb titers necessary to achieve protection. These protective ranges are indicated in Figures 4A and 4B, to demonstrate the putative protective capacity of the immunization against different variants.

We first measured the protective capacity (NAb titers) of human-vaccinated antibody responses against the different variants (Fig. 4A). As previously described[46-48], serum samples from individuals vaccinated with BNT162b2 (encoding ancestral strain full-length-Spike, two doses, not boosted) neutralized pseudotyped viruses encoding Beta, Delta, Gamma, and Omicron spikes with reduced efficiency compared to the neutralizing activity against the spike from the ancestral variant (Fig. 4A). Based on the defined protective range, serum from vaccinated individuals were protective against the ancestral and Gamma SARS-CoV-2 variants, while the neutralizing efficacy against the highly divergent Omicron BA.1 variant was considerably reduced (Fig. 4A)[49]. As expected, VAANZ-Δ_RRN showed a strong response against the ancestral and Delta variants. Interestingly, mice immunized with VAANZ-Δ_RRN had high levels of cross protective antibodies against Beta and Gamma and even Omicron BA.1 SARS-CoV-2 variants.

We also observed a marginal increase in NAb titers versus SARS-CoV from VAANZ-Δ_RRN vaccinated mice compared to NAb titers from PBS controls (Fig. 4B). In summary, these data suggest that VAANZ-Δ_RRN protein vaccine induced cross-reactive NAbs to a number of SARS-CoV-2 variants of concern, including the ~~highly diverse~~ antigenically distinct Omicron BA.1.

Given the evident breadth of the antibody response generated by VAANZ-Δ_RRN, we investigated the mechanism by which this subunit vaccine provides broad protection. Figures 3C to 3I demonstrate the benefit of including the NTD in the "cognate" response against the Delta variant, therefore we sought to address the role of the NTD in the generation of cross-protective antibodies. We hypothesized that the incorporation of the NTD could improve cross-reactive immunity through two distinct mechanisms. Firstly, the additional T cell epitopes provided by the NTD could support the GC response to enhance B cell activation and the production of high quality antibodies[50]. Secondly, the NTD itself expresses epitopes for NAbs [11,12], and therefore, could increase the breadth of the NAb response. To address this hypothesis, we focused on two variants, Beta B.1.351 and Omicron BA.1, which are known to contain escape mutations, yet were still recognized by NAb from VAANZ-Δ_RRN immune sera (Fig. 4B).

Firstly, to determine whether vaccination with VAANZ-Δ_RRN promoted higher quality anti-RBD antibodies that could explain the observed cross-neutralization activity, we compared antibody affinity to serum from Δ_RBD-RBD immunized mice. We observed that vaccination with VAANZ-Δ_RRN generated higher affinity anti-RBD antibodies than immunization with the Δ_RBD-RBD protein (Fig. 4C) suggesting that inclusion of the NTD, and the associated increased frequency of T_{FH} cells (Figs. 3E to 3G) improved affinity maturation. Next, we established a

surrogate virus neutralization test (SVNT) with RBD proteins from Omicron BA.1.1.529 and Beta B.1.351 SARS-CoV-2 variants to determine whether higher affinity anti-RBD targeting antibodies exhibited enhanced cross-neutralizing activity. Interestingly, we observed a mixed result that was dependent on the virus variant (Fig. 4D). Higher affinity antibodies induced by VAANZ-Δ_RRN immunization promoted an increased neutralization activity against the Beta B.1.351 variant, but no difference was observed against the Omicron BA.1.1.529 variant compared to Δ_RBD-RBD immune serum. This data suggests that higher Ab affinity can help improve cross-reactivity but will depend on the extent of the mutations within the spike protein of the virus variant. To determine whether immune serum from VAANZ-Δ_RRN had a greater capacity to neutralize the Omicron BA.1 variant compared to NAb response induced by Δ_RBD-RBD immunization, we evaluated the capacity to neutralize a SARS-CoV-2 Omicron BA.1 spike pseudotyped virus. Notably, the incorporation of the NTD did improve neutralization activity, showing higher NAb titers from VAANZ-Δ_RRN immunized serum compared to serum from Δ_RBD-RBD immunized mice (Fig. 4E). Since anti-RBD-targeting Abs from VAANZ-Δ_RRN and Δ_RBD-RBD vaccinated mice showed equivalent activity against the Omicron BA.1 variant, we reasoned that enhanced neutralization capacity observed in the SARS-CoV-2 spike pseudotyped virus neutralization assay would be due to antibodies targeting the NTD. We assessed the extent of NTD targeting by NAbs, by comparing the ratio of S1 (expressing epitopes on RBD and NTD) NAb to RBD NAbs specific for Omicron BA.1 variant. As expected, NTD targeting was greater for serum from mice immunized with VAANZ-Δ_RRN (Fig. 4F). These data suggest that there are conserved epitopes on the NTD between SARS-CoV-2 variants of concern that can be targeted by immunization with VAANZ-Δ_RRN and are critical for ~~protection against~~ neutralization of the Omicron BA.1 variant. In summary, improved cross-protection provided by VAANZ-Δ_RRN was

mediated via two independent mechanisms, increased Ab potency and broader NAb response. Of note, the dependency on these separate mechanisms was dictated by the virus and the extent of amino acid changes and conserved epitopes expressed by the SARS-CoV-2 variant.

We confirmed the cross-protective capacity of our vaccine candidate with a heterologous challenge model. We focused on the Beta B.1.351 variant, as the Omicron BA.1 does not cause severe disease in mice. As in Figure 2A-D, mice were immunized with 50 μg of VAANZ-Δ_RRN, or as a positive control given a sub-lethal dose inoculation of 10^2 $TCID_{50}$ SARS-CoV-2 (SARS-CoV-2/Australia/Vic/01/20 (ancestral strain–like) on day 14. On day 35, all groups of mice were intranasally challenged with 1 x 10^4 $TCID_{50}$ of SARS-CoV-2 (SARS-CoV-2/Australia/QLD/1520/2020 (B.1.351 Beta variant)) and then monitored for body weight changes and mortality. Similar to the convalescent group, we observed no weight loss and 100% survival in the immunized group. Similarly, no live virus was detected in the lung or nasal turbinate of immunized mice following challenge (Figure 4E). Therefore, RBD-RBD-NTD protein subunit vaccine provides protection against diverse viral variants.

DISCUSSION

There is still a need for an effective booster vaccine that prevents COVID-19 disease by emerging SARS-CoV-2 variants. RBD proteins are promising targets as they contain neutralizing epitopes, focusing the immune response to protective determinants that cross-neutralize multiple variants of concern. Here, we describe a novel RBD-based protein vaccine (VAANZ-Δ_RRN) that is highly immunogenic, expresses well, and has a good stability profile. We showed that the incorporation of an NTD significantly enhanced the breadth of the T cell response, resulting in increases in both the T_{FH} and IFN-γ^+ T cell response. Increased T cell responses correlated with

improved antibody function. In particular, immunization with VAANZ-Δ_RRN increased cross-protective NAbs, including reactivity to the highly divergent Omicron BA.1 variant. Importantly, VAANZ-Δ_RRN provided equivalent protection in mice to that seen in convalescent mice. Together, these data suggest that VAANZ-Δ_RRN is a good candidate for a booster vaccination and may provide more efficient protection against SARS-CoV-2 variants of concern compared to the less complex RBD-based vaccines and drive an NAb-enriched boosted response compared to full-length spike-based vaccines.

RBD-based vaccines have been shown to be as immunogenic as the full-length SARS-CoV-2 spike protein[51], with the added benefit of reducing the risk of eliciting non-neutralizing, potentially detrimental Abs[52-56]. To date, 11 RBD-based COVID-19 vaccines have been approved for use[57], none of which contain additional domains from the spike protein. Our unique design was engineered with a reverse orientation which allowed for high production of 0.5 g/L through single clone selection. A vaccine's potential to cross-react to novel SARS-CoV-2 variants is key to controlling the COVID-19 pandemic**.** Here we showed that vaccination with VAANZ-Δ_RRN generated antibodies that cross-react with SARS-CoV-2 ancestral, Beta, Gamma and Omicron-BA.1 variants. We also showed that the incorporation of the NTD not only improves T cell immunity, antibody and B cell memory responses to the Delta variant, but also promoted a superior cross-protective response compared to the RBD tandem dimer. Our investigations revealed that improved Ab potency as well as additional anti-NTD NAbs contribute to enhanced cross-protection. Of note, the enhanced capacity to cross-react, largely depended on the viral variant and the mutations they possess. Therefore, the advantage of incorporating the NTD was two-fold,

leading to a better ability to generate immune responses that may protect against a wide range of SARS-CoV-2 variants of concern.

In addition to maintaining immunity in the face of viral evolution, vaccines must also ensure immune durability. Natural immunity in convalescent individuals has been shown to decline at a rapid pace[58] and Abs induced after two shots of a COVID-19 vaccine wane after only a few months [59]. Our longevity studies in mice show that antibody titers from immune serum from NTD-RBD-RBD protein vaccination are maintained at a stable level for at least 8 months. Like immunization with BNT162b2, we also observed waning titers after 9 months[59]. However, the mice were approaching an "aged" state at the 9 month post vaccine timepoint, which has been associated with several immunological defects[60] and could confound antibody durability measurements. Determining the factors that promote long-lived antibody to the RBD is currently the subject of intense research.

Antiviral T cell immunity also contributes to protection against SARS-CoV-2, mostly through mechanisms to prevent disease severity and reduce morbidity and mortality[61-65]. Studies in mice that lack B cells[66], or humans with waning antibody responses[21,58,67,68] have demonstrated the important role for T cells in maintaining cross-protective immunity. Epitope mapping using overlapping peptides in convalescent humans have shown that both the RBD and NTD contain a number of immunodominant $CD4^+$ and $CD8^+$ T cell antigens and are conserved between variants[69], suggesting that the RBD and NTD are more than adequate for inducing antiviral T cell responses following vaccination. Moreover, our data show that the inclusion of the NTD increases the size of the T cell response by at least 4-fold compared to T cell responses in mice immunized with the

RBD tandem dimer protein. Thus, the superior T cell response induced by VAANZ-Δ_RRN could be beneficial for protection against severe disease by emerging variants, especially if variants contain immune escape mutations.

As the pandemic endures, and SARS-CoV-2 variants continue to spread while human immunity wanes, booster vaccines will be required. The current public health advice in many countries is to offer a third dose of homologous vaccine to all individuals, and even a fourth dose to those who are considered highly vulnerable. While this strategy increases the frequency and breadth of antibodies overall, it does not specifically amplify NAbs for new variants of concern [16,33]. The focused approach laid out here is better suited for future variants than whole spike approaches. Firstly, because 99% of NAb from FL-spike vaccinated serum targets the RBD[70], and secondly, to avoid the risk of inducing unwanted Abs that are potentially detrimental. Future work will assess the capacity of this subunit vaccine to provide protection against new emerging variants. Work is also currently progressing to test VAANZ-D_RRN vaccine safety and efficacy in a phase I/II clinical trial.

Limitations of Study

It is important to note that using mouse models to assess T cell immunity possess several limitations. In our study, antigen-specific T cells were only assessed by ELISpot assays re-stimulated with overlapping peptide pools from the spike protein, rather than discrete T cell peptide antigens. While these assays are highly sensitive and can measure a functional cytokine response, they do not distinguish between $CD4^+$ and $CD8^+$ T cells. Therefore, we cannot make conclusions on the contribution of each population. Secondly, because mice and humans express unique T cell

repertoires, the proportion and ratio of $CD4^+$ to $CD8^+$ T cell response is likely to be different. Therefore, data from these mouse studies can be interpreted as a "proof of principle" to assess the general role of T cells in the immunogenicity of RBD-based vaccines.

Consortia: In addition to the named authors, the following individuals are members of the VAANZ group, who have provided input into development of the protein candidate: Shivali A. Gulab And Peter Kelly (Avalia Immunotherapies, Wellington, New Zealand); Bethany Andrews, Frances Priddy (Malaghan Institute of Medical Research, Wellington, New Zealand); Lee Law and William Rolleston (South Pacific Sera, Ltd, Timaru, New Zealand); Gavin Painter (Victoria University of Wellington, New Zealand).

Acknowledgments: We thank Prof. Alessandro Sette and Prof. Shane Crotty, La Jolla Institute for Immunology, La Jolla, USA for consultation and critical discussion on T cell epitopes from the SARS-CoV-2 N Terminal Domain. We also thank Prof. Franca Ronchese and Prof. Graham Le Gros, Malaghan Institute of Medical Research, Wellington, New Zealand, and Dr Shivali Gulab and Dr Peter Kelly, Avalia Immunotherapies, Wellington New Zealand for critical discussion. We thank Dr. Reed Johnson, Dr. Bernard Lafont and Nicole Lackemeyer (SCV2 Virology Core, NIAID, MD) for generation of viral stocks used for murine challenge studies. We thank Malaghan Institute Biomedical Research Unit and NIAID Animal Facility Staff for animal care. We thank Hugh Green Cytometry Core for technical assistance. We thank Dr. Julian Druce from the Victorian Infectious Diseases Reference Laboratory (VIDRL) for providing SARS-CoV-2 isolates (SARS-CoV-2/Australia/Vic/01/20 (ancestral; Wuhan-1 like SARS-CoV-2)), SARS-CoV-2/Australia/Vic/18440/2021 (Delta) and SARS-CoV-2/Australia/QLD/1520/2020 (B.1.351; Beta)

used in this study. We thank Rebecca Plavcak and Charley Mackenzie-Kludas for technical support for during the murine studies conducted at the Doherty Institute.

Funding: COVID-19 Innovation Acceleration Fund, Ministry of Business, Innovation & Employment (MBIE), New Zealand, and the Addressing Security of Supply for a SARS-COV-2 Prophylactic Vaccine for New Zealanders, New Zealand (MALA2001) Intramural Program of NIAID, NIH, United States.

Author contributions: Conceptualization: IS, LMC, DC, MEQ-M

Methodology: IS, LMC, DC, MEQ-M

Investigation: IS, OP, NM, TP, AA-H, LMC, (immunogenicity); DC, TWB, NMM, GM, SM (mammalian protein production); GM, EJP (yeast protein production); RH, LCH, BL, JK, SS, MEQ-M (virology), KLH, AS, DEA, KS (challenge studies)

Visualization: IS, LMC, DC, MEQ-M

Funding acquisition: JEU, IH, LMC, DC, MEQ-M

Project administration: LMC

Supervision: LMC, DC, MEQ-M

Writing – original draft: IS, MEQ-M, DC, LMC

Writing – review & editing: JEU, IFH

Declaration of interests: The authors declare no conflict of interests, other than the filing of patent application number AU2021902667 entitled “Fusion Polypeptide”. The funders had no role in the design of the study; in the collection, analyses, or interpretation of data; in the writing of the manuscript, or in the decision to publish the results.

Data and materials availability: Raw data can be requested by contacting the corresponding authors.

Institutional review board statement: The study was conducted according to the guidelines of the Declaration of Helsinki and approved by the University of Otago Human Ethics Committee (protocol H21/134) All experiments involving replication-competent SARS-CoV-2 were performed under the auspices of the Institutional Biological Safety Committee (IBSC) at either University of Otago or University of Melbourne, in an approved BSL-3 facility. Protocols for virus inactivation were approved by the IBSC. Work with inactivated SARS-CoV-2 and SARS-CoV-2 spike pseudotyped viruses was performed in a BSL-2 laboratory.

Figures

Fig. 1. Development of novel SARS-CoV-2 subunit vaccine. (**A**) Schematic drawing of the spike protein of SARS-CoV-2. S, signal peptide; NTD, N-terminal domain; RBD, receptor binding domain; TM transmembrane domain. Numbers refers to the amino acid position in the spike protein. (**B**) Cartoon of VAANZ-W_RRN construct showing the position of the tags, the antigenic domains, and the cleavage points. L, leader sequence; F, FLAG tag; Fc,

human Fc domain of IgG1; scissors are the location of the HRV-3C protease cleavage sites (**C**) Summary of the RBD proteins produced. Virus variant, mutations present, length in amino acids and theoretical mass (kDa) are reported.

Fig. 2. Protection following immunization with VAANZ-Δ_RRN is equivalent to protection from previous infection. (**A**) Schematic of immunization and SARS-CoV-2 challenge protocol. K18-hACE2 transgenic mice were either unvaccinated, immunized with **VAANZ-Δ_RRN** or challenged with sublethal dose of ancestral SARS-CoV-2. All mice groups received 1 x 10^4 $TCID_{50}$ of SARS-CoV-2 on Day 35 and monitored for weight loss (**B**) and survival (**C**) for 16 days post infection. Viral titers from lung and nasal turbinates at day 3 post infection (**D**). Symbols and error bars indicate mean ± SD from groups of 10 as shown in C. P values were calculated by a Mixed-effect analysis (B) or Mantel-Cox Log Rank test (C), each group were compared to unvaccinated controls. (**E**) Anti-RBD IgG in sera over time from C57BL/6 mice immunized with VAANZ-Δ_RRN /AddaVax or 6 μg of inactivated SARS-CoV-2 virus/AddaVax. Symbols indicate geometric mean ± SD from groups of n=10. Mice were immunized with 2 doses of PBS or 50 μg of specified protein vaccine and AddaVax, spaced 3 weeks apart and assessed 1 week after the second dose. All data are pooled from 2 independent experiments. P values in D-E were calculated by one-way ANOVA with Tukey's multiple comparison. **, $P < 0.01$; ****, $P < 0.0001$; ns, not significant.

Fig. 3. VAANZ-Δ _RRN induces stronger immune responses than Δ_RBD-RBD vaccine. Responses to VAANZ-Δ_RRN were compared to Δ_RBD-RBD. (**A**) RBD-specific and S1-specific IFNγ producing cells and their ratio (**B**) is shown. (**C**) Plots gated on $CD4^+CD44^+TCRb^+$ cells show T_{FH} CD4 T cells expressing PD-1 and BCL6. Percent among $CD4^+$ cells (**D**) and number (**E**) of T_{FH} cells. Anti-RBD IgG (**F**) and S1-binding B cells (G-J) were measured. (**G**) S1-specific tetramer on IgD^-B220^+ cells. $S1^+B$ cells as total number (**H**) number within subset (**I**) and (**J**) percent among B cell subset. Data are pooled from 2-3 independent experiments, symbols indicate individual mice from groups of n = 5-10. Bars indicate mean (except in B and H) or geometric mean (B, H). P values were calculated by one-way ANOVA with Tukey's multiple comparison, except in A, I-J, which were calculated by two-way ANOVA *, $P < 0.05$; **, $P < 0.01$; ****, $P < 0.0001$.

Fig. 4. Enhanced breadth of antibody neutralization generated by VAANZ-Δ_RRN compared to Δ_RBD-RBD. Mice were immunized as in Fig. 3 legend. Comparison of pseudotyped lentivirus neutralization antibody titers against SARS-CoV-2 variants from (**A**) human sera of individuals immunized with BNT162b2 or (**B**) serum from mice immunized with VAANZ-Δ_RRN. Blue line shows geometric mean ± SD ID_{50} of human BNT162b immunized serum, pink line shows geometric mean ± SD ID_{50} of mouse serum immunized with VAANZ-W_RRN, both against ancestral variant. (**C**) Antibody

dissociation assay was performed to calculate affinity index of anti-RBD IgG from VAANZ-Δ_RRN and Δ_RBD-RBD immunized mice. (**D**) Inhibition of interaction between RBD (from Omicron BA.1 and Beta variants) and hACE2 by sera from immunized mice. (**E**) Pseudotyped lentivirus neutralization antibody titers (ID_{50}) against Omicron BA.1 variant. (**F**) NTD targeting antibodies were measured as a ratio of S1-ACE2 and RBD-ACE2 SVNT antibody titers (IC_{50}). K18-hACE2 transgenic mice were either unvaccinated, immunized with **VAANZ-Δ_RRN** or challenged with sublethal dose of ancestral SARS-CoV-2. All mice groups received 1 x 10^4 $TCID_{50}$ of Beta variant SARS-CoV-2 on Day 35 and monitored for weight loss (**B**) and survival (**C**) for 16 days post infection. Viral titers from lung digests and nasal turbinates at day 3 post infection (**D**). Box plots in A-B show median, upper and low quartile range and outliers. Bars in C-F indicate geometric means from groups n = 5-10 mice pooled from 2 independent experiments. P values were calculated by one-way ANOVA with Tukey's multiple comparison **, $P < 0.01$; ****, $P < 0.0001$; ns, not significant.

STAR METHODS

Resource availability

*Lead Contact***.** Further information and requests for resources and reagents should be directed to and will be fulfilled by the lead contact, Lisa Connor (Lisa.Connor@vuw.ac.nz)

*Materials Availability***.** All plasmids are available on request and require MTA for transfer.

Data and code availability. Any additional information required to reanalyze the data reported in this paper is available from the lead contact upon request.

Experimental model and subject details.

*SARS-CoV-2 challenge studies in mice***.** Sex matched B6.Cg-Tg (K18-ACE2)2PrImn/J hemizygous six- 12-weeks of age were purchased from The Jackson Laboratory (NIH challenge studies) or Animal Resources Centre, Australia (University of Melbourne challenge studies). Ancestral strain experiments were performed at NIAID/National Institutes of Health. B.1.351, Beta variant; B.1.617.2 Delta variant challenge studies were performed at AgriBio, Centre for AgriBioscience, Bundoora, Australia. All challenge studies were performed in accordance with institutional guidelines approved by the respective Animal Ethics committees; Animal Care and Use Committee at the NIAID/National Institutes of Health (SARS-CoV-2 WA1/2020 challenge studies) or University of Melbourne Animal Ethics Committee, University of Melbourne (B.1.351, Beta variant; B.1.617.2 Delta variant challenge studies). All animal experiments were conducted in a certified Physical Containment Level 3 (PC3) facility.

Immunogenicity testing in mice. Specific pathogen-free mice were bred and housed at the Malaghan Institute of Medical Research. C57BL/6J mouse breeding pairs were originally obtained from The Jackson Laboratory. Sex-matched mice between 6-12 weeks of age were used for all experiments and mice were age-matched within 2 weeks of each other in any given experiment.

Study approval. Mouse studies: Experimental protocols were approved by the Victoria University of Wellington Animal Ethics Committee (28569) or by the Animal Welfare committee at the University of Melbourne and experiments were carried out in accordance with their guidelines (20763). Human studies: Written informed consent was received for ten participants who had received two doses of Pfizer (BNT162b) vaccine, as part of the VAANZ Vaccine Study

(sub study of Healthy Donor Tissue for Immune System Research) with approval from the Health and Disability Ethics Committee (Ref # 21/CEN/227). Participants were between the ages of 20 and 60 years, and a mix of male and female.

Method Details

Gene synthesis. The cDNA insert of each SARS-CoV-2 construct was codon optimized for human cell expression, synthesized and sequence-verified by Gene Universal (Geneuniversal.com), and cloned via 5' *Not*I and 3' *Xba*I restriction sites into a modified pCMV6-XL4 vector in frame with an N-terminal DYKDDDDK peptide and a C-terminal human Fc fragment [71]. Both tags were cleaved by HRV-3C protease (LEVLFQ/GP) (made in house) during the purification process. See Figure 1 for a schematic of the construct and the domain boundaries.

Generation of stable cell lines for protein production. HEK293 cells lacking N-acetylglucosaminyltransferase I (GnTI-) activity (HEK293 GnTI-) were obtained from American Type Culture Collection (ATCC, Manassas, VA). Protein made in these cells only contain a Man5GlcNAc2 [72] to each N-linked glycosylation site, thus leading to a more uniform epitope availability. HEK293 GnTI- cells were cultured in DMEM supplemented with 5% FBS at 37°C and 5% CO_2. Stable cell lines were made for all constructs by selecting for resistance to Geneticin (G418) (Sigma) using DMEM supplemented with 5% FBS and 500 µg/ml of G418. Resistant clones were isolated using Pyrex cloning rings (Merck) and stable expression of the proteins was tested by western blot using anti-FLAG antibody (M2) (Sigma). Clones expressing high levels of the protein were amplified, frozen, and used in large-scale protein production.

Protein expression and purification. Milligram-scale protein production was performed in triple layer cell culture flasks or with Bellocell (Cesco Bioengineering, Taiwan) depending on the desired yield, with regular collection and replenishment of the cell culture medium containing 2-5% FBS. Typically, 2-5 L of conditioned medium was collected for purification. Proteins were affinity purified from cell culture media using Protein A- CaptivATM PriMAB (RepliGen, Waltham, MA) in 150 mM NaCl, 20 mM Tris, pH 8.0 or anti-FLAG® M2 affinity resin (Sigma), and subsequently cleaved with HRV 3C protease (made in house) to remove the FLAG and Fc fragments. Residual HRV 3C protease and Fc fragments were removed from the protein of interest by a coupled negative purification step using HiTrap MabSelect PrismA – GSTrap™ HP (Cytiva) in PBS. The protein was used within a week or aliquoted and flash frozen in liquid nitrogen and stored at -80°C. To purify full fusion proteins for downstream experiments, when it was beneficial to maintain the Fc tag (e.g. ELISA, Biolayer interferometry or BLI), affinity chromatography was used with anti-FLAG® M2 affinity resin to capture the DYKDDDDK peptide. The saturated resin was washed in PBS and eluted in PBS containing the DYKDDDDK peptide at 0.1 mg/mL. The eluted protein was concentrated using centrifugal concentrators with the appropriate molecular weight cut-off (Pall) and used within a week or flash-frozen in liquid nitrogen and stored at -80°C until needed.

Production of yeast derived protein. Generating pure RBD for antibody binding assays broadly followed the method described for SARS-CoV RBD [73]. Pichia pastoris strain KM71H transformed with construct pPICZα-RBD encoding for ancestral SARS-CoV-2 spike, residues 333-530, was used to express and secrete the RBD. Expression was performed in BMM medium (1.34% w/v YNB, 0.00004% w/v Biotin, 1% v/v methanol, in 100 mM potassium phosphate, pH 6.0) at 30°C

and 280 rpm over the course of 2-3 days with intermittent refeeding (1% v/v methanol) after 24 hours. The clarified (0.2 μm PTFE membrane) expression medium containing the secreted protein was prepared for Hydrophobic interaction chromatography by adding solid $(NH_4)_2SO_4$ to 2 M. The RBD protein was captured on a HiTrap Butyl Sepharose HP column (Cytiva) and eluted using a stepwise gradient from 20 mM Tris, 2.0 M $(NH_4)_2SO_4$, pH 8.0 to 20 mM Tris, 0.02 M $(NH_4)_2SO_4$, pH 8.0. The resulting preparation was polished on a HiLoad 16/600 Superdex 200 pg column (Cytiva) using PBS. After elution, endotoxin was removed employing Polymyxin B agarose (Sigma Aldrich).

*Protein size exclusion chromatography***.** Aggregation, oligomerization or other in-solution behaviour was monitored by size exclusion chromatography using either a Superose 6 Increase 10/300 GL or a HiLoad 16/600 Superdex 200 PG column equilibrated in PBS (Supp. Fig. 1). If aggregation was present, the fractions corresponding to the soluble protein were collected and re-concentrated, the protein concentration measured, and the protein flash frozen.

Thermal stability assay. Solutions of 10 μM of protein sample in a final volume of 20 μL per well were prepared by mixing 2.5 μL of 50x SYPRO Orange [74] (Sigma) that was initially prepared from a 5000x solution with protein in 50 mM Tris, pH 8; 150 mM NaCl or PBS (1x), pH 7.4 and loaded into MicroAmp™ Fast Optical 48-Well Reaction Plate (ThermoFisher SCIENTIFIC), sealed with optical-quality sealing tape (ThermoFisher SCIENTIFIC). Thermal denaturation was performed using a 48-well StepOne™ Real-Time PCR System (ThermoFisher SCIENTIFIC) where temperature was increased in a step-wise manner from 10°C to 95°C in 0.2°C/cycle

increments (ramp rate of ~0.6°C/min) and with an equilibration time of 5 seconds at each temperature.

RBD-ACE2 binding assay. Binding between the generated Fc constructs and ACE2-alkaline phosphatase (AP) fusions was assessed by Enzyme-linked immunosorbent assay (ELISA) [71]. A 3 µg/mL solution of mouse anti-AP (PLAP Ab-1 (8B6.18) Mouse monoclonal, NeoMarkers) in PBS was added to the wells of 96-well plates, sealed and incubated overnight at 4°C. Plates were washed three times with 200 µL/well of PBS and 0.05% Tween and then blocked with 5% food grade non-fat dry milk (Alpine) in PBS for 1 hour at RT. 20 µL of ACE2-AP conditioned medium containing 2 µL of monoclonal mouse anti-human IgG1-HRP (Bio-Rad) was added to each well along with 20 µL of decreasing concentrations of each purified candidate protein-Fc, from 100 nM to 0.01 nM in 3-fold dilutions, plus buffer only. Plates were sealed and incubated for 4 hours at RT in the dark. Plates were washed as above, and 15 µL 1-Step Ultra TMB-ELISA HRP (ThermoFisher) substrate was added and incubated for 1 hour at RT. Plates were read at the absorbance of 650 nm using a microplate plate reader. Positive control (NRXN1-AP binding to NLGN1-Fc) was used to ensure the assay was working and a negative control (No AP-ACE2 on the plate) was used to obtain background values to quantify the positive reactions.

Immunizations in mice. For all immunizations except those performed at UoM mice were anesthetized by intraperitoneal injection of Ketamine and Xylazine solution (ProVet NZ). All mice were immunized by intramuscular injection on both legs, each injection containing 50 µL per leg with equal volume of antigen and adjuvant. Mice were immunized twice, three weeks apart, and both immunizations included either inactivated SARS-CoV-2 virus (NZ/Queenstown/01) at 6 µg

per mouse, or RBD protein candidates at 50 μg per mouse, with AddaVax™ adjuvant (Invivogen). The dose refers to the total amount of antigen injected per animal.

SARS-CoV-2 challenge studies in mice stock production was performed in VeroE6/TMPRSS2 cells cultured in DMEM supplemented with GlutaMAX and 2% FBS under BSL-3 conditions. Culture supernatant and cells were collected and clarified by centrifugation 48 hours after inoculation. Supernatant was then collected, aliquoted and frozen at -80°C. Virus titers were determine by $TCID_{50}$ assay in Vero E6 cells (CRL-1586; American Type Culture Collection) using the Reed-Muench calculation method [75]. Whole genome sequencing of the SARS-CoV-2 WA1/2020 virus stock was performed at the NIAID Genomic Core (Rocky Mountain Laboratories, MT). SARS CoV-2 infections were performed under BSL3 containment. Four SARS-CoV-2 strains were used in this study, including (1) SARS-CoV-2/WA/2020 (2) SARS-CoV-2/Australia/Vic/01/20 (ancestral strain–like), (3) SARS-CoV-2/Australia/Vic/18440/2021 (B.1.617.2; Delta), and (4) SARS-CoV-2/Australia/QLD/1520/2020 (B.1.351; Beta). The WA/2020 stock used for challenge experiments contained two single nucleotide polymorphisms when compared to the reference sequence (MN985322.1): 26542 T7I (M) and 28853 S194T (N). Virus was propagated in Vero-TMPRSS2 cells cultured with DMEM supplemented with 5% fetal bovine serum (FBS) and 1% P/S at 37°C, 5% CO2. Cell culture supernatants were harvested, centrifuged and aliquoted once cytopathic effect (CPE) was observed. Viral titres were determined by limited dilution using the Karber method [76].

Animals were anesthetized by isoflurane inhalation, and either 10^2 (sublethal dose, to establish convalescent group) or 1×10^4 $TCID_{50}$ of SARS-CoV-2 was administered by intranasal instillation

variants in a maximum volume of 50 µL. After infection, mice were monitored daily for clinical signs.

Virus Quantification. Lungs and nasal turbinates were homgenized in 2 mL and 1 mL of PBS, respectively. Vero-TMPRSS2 cells were infected to determine the tissue culture infective dose ($TCID_{50}$/ml). Vero- TMPRSS2 cells in 96-well plates were utilized for titration assays. Samples (virus and homogenised tissue) were serially diluted in DMEM, supplemented with 5% FBS and 1% penicillin/streptomycin. Cells were infected with 100 µL of diluted sample in quadruplicate. Cells were incubated at 37°C and 5% CO_2 for 5 days. Following incubation, wells with CPE were recorded and the virus titre ($TCID_{50}$/mL) for each sample determined by limited dilution using the Karber method.Virus titers are expressed as $TCID_{50}$ per mL

Preparation of tissues for immunological assessment. C57BL/6 mice were sacrificed, and blood, spleens, and both inguinal lymph nodes (iLNs) were collected for analysis. Blood was obtained via cardiac puncture, collected into S-Microvette® serum gel tubes (Sarstedt) before centrifugation at 10,000 x g for 5 minutes and serum was decanted, aliquoted and frozen at -80°C. Single cell suspensions of splenocytes were prepared by teasing spleens through a 70 µm cell strainer (Falcon®) and washing through with Iscove's Modified Dulbecco's Medium (IMDM) (Gibco) before centrifugation at 250 x g for 10 minutes. Cell pellets were resuspended in red blood cell lysis solution (Qiagen) and cells were centrifuged at 300x g for 4 minutes before resuspension in R10 media (Roswell Park Memorial Institute [RPMI] 1640 Medium [Gibco] supplemented with heat inactivated 10 % FBS [Gibco]) and filtered through a 70 µm cell strainer. Single cell suspensions of iLNs were prepared by teasing through a 70 µm cell strainer and washing through

with IMDM. Cells were then centrifuged at 250 x g for 10 minutes before resuspension in R10. Cell numbers were enumerated using SPHERO Accucount Blank particles (Spherotech) according to the manufacturer's protocol.

Human serum sample collection. The average time between immunization with second dose of BNT162b and sample collection was 166 days. Between 80 to 100 mL of peripheral blood was collected from each participant. Samples were incubated at RT for 30 minutes and centrifuged at 2000 x g for 10 minutes at 4°C. Serum layer was collected and stored at -80°C for pseudotyped virus neutralisation assays.

Flow cytometry. Prior to staining, cells were incubated with anti-mouse CD16/32 (clone 2.4G2, affinity purified from hybridoma culture supernatant) at RT for 5 minutes. Dead cells were identified and excluded from analysis using Zombie NIR fixable viability kit (BioLegend) according to manufacturer's instruction. For staining of cell-surface molecules, cocktails of fluorescent antibodies in Flow cytometry buffer (PBS with 0.01% sodium azide, 2 nM EDTA, 2% FCS) were applied at 4ºC for 15 minutes. Cells were then washed with 4 mM biotin PBS and stained on ice for 30 minutes with RBD-SAv tetramers. Cells were fixed and permeabilised with eBioscience™ FoxP3/transcription factor fixation/permeabilization concentrate and diluent (Invitrogen), according to the manufacturer's protocol, and then labelled with intracellular antibodies at RT for 1 hour. Details on Individual fluorescently conjugated antibodies are presented in Table S1.

B cell tetramer production. Protein-biotin conjugates were prepared with SARS-CoV-2 S1 domain (S1) and ovalbumin (OVA) protein. Separate reactions were set up to add two fluorescently labelled streptavidin (SAV) to RBD and OVA. SAV was added at a 1:50 protein to SAV ratio. One fifth of the fluorescently labelled SAV was added to the protein at a time, with 20-minute incubations between applications, on ice. When all the SAV was added, 4 mM free biotin (Sigma) in PBS was added at a 1:1 volume ratio, to saturate free SAV. The tetramers were then spun at max. speed at 4^{o}C for 30 minutes. Specific cells were identified as OVA negative, S1 positive.

All samples were collected on a Cytek® Aurora spectral flow cytometer (Cytek®). Compensation was performed in each experiment using UltraComp eBeads (Invitrogen). Analysis was performed using FlowJo version 10 (BD biosciences).

*Interferon Gamma (IFN-γ) ELISpot***.** Mouse anti-IFN-γ ELISpot kit (Mabtech) was used according to the manufacturer's instructions. Briefly, plates pre-coated with mouse anti-IFN-γ mAb AN18 (Mabtech) were washed and conditioned with R10 media according to the manufacturer's protocol. Splenocytes were plated at 3 x 10^5 cells per well in R10 containing PepMix™ peptide pools (JPT) at a final concentration of 0.5 μg/mL and were incubated at 37°C for 18 hours. Negative control wells (media only) and positive control wells containing PMA at 2.5 ng/mL and ionomycin at 1 μg/mL were included for each sample. Spots were enumerated using an AID ELISpot reader and software. To generate normalized readings, spots in negative controls were subtracted from corresponding test wells and counts were presented as spot-forming units per million splenocytes.

ELISA based assays

Conventional ELISA:Nunc MaxiSorp™ 96-Well ELISA Microplates (ThermoFisher) were coated with 100 µL of 2 mg/mL RBD in carbonate buffer (0.1M Sodium bicarbonate and sodium carbonate) overnight at 4°C. RBD protein was expressed in a yeast system, as previously described[73]. Plates were washed 3 times in PBS and 0.05% Tween and then blocked with PBS and 10% FBS for 1 hour at RT. Serum samples were initially diluted to 1:100, and then serially diluted at 1:10 in PBS and 10% FBS. For negative controls, four wells/plate contained 10% FBS (blank) and four wells/plate had serum (diluted to 1:100) from PBS treated animals. For a positive control, 10 ng/mL of monoclonal mouse anti-spike IgG1 clone 43 antibody (SinoBiological), was added to the first row of one column and serially diluted at 1:10. Plates with serum samples were incubated for 2 hours at RT. The plates were washed as before and 1 mg/mL goat anti-mouse total IgG HRP (Invitrogen), diluted in PBS and 10% FBS was added and incubated for 1 hour at RT. Plates were washed 3 times with PBS and 0.05% Tween before addition of 100 µL/well of 1:1 TMB A and B substrate solution (OptEIA™ substrate reagent set, BD Biosciences) The reaction was stopped with 50 µL 2M H_2SO_4 and plates were read at 450 nm on a Perkin Elmer EnSpire 2300 multilabel plate reader. The end point titer was calculated using the *t*- statistic method [77].

Binding affinity assay*:* To evaluate the affinity of antibodies specific for RBD, the same protocol for conventional ELISA was used, however a dissociation step was included to remove low affinity antibodies. Diluted serum samples were plated in technical replicates for two conditions; standard and urea treated (used to dissociate low affinity antigen-antibody binding). As above, plates were incubated with serum samples for 2 hours at RT and washed 3 times in PBS and 0.05% Tween. For dissociation condition, 6 M of urea (Sigma) was added to wells whereas

PBS was added to wells of the standard condition. Plates were incubated at 37°C for 30 minutes and then immediately dowsed with PBS and 0.05% Tween to stop the reaction. Detection of antibody binding was performed using the conventional ELISA methods. The affinity index was calculated as the signal detected in the urea condition as a percentage of the standard condition signal, at the dilution where the standard signal is at 80% of the max signal. This was selected as the "dilution of interest" to ensure loss of signal was observed within the "linear" section of the sigmoidal curve, and not when the antibody was saturating.

Surrogate Virus Neutralization Test (SVNT): Nunc MaxiSorp™ 96-Well ELISA Microplates (ThermoFisher) were coated with 100 µL of 2 mg/mL ACE2-Fc in carbonate buffer overnight at 4°C. Plates were washed with PBS and 0.05% Tween and blocked with 20% FBS for 1 hour at RT. Serum samples were initially diluted to 1:5, and then serially diluted at 1:4 in PBS and 20% FBS. In a separate plate 30 µL of diluted serum was added to 30 µL of 2x Kd RBD-HIS (Sino Biological), and incubated for 2 hours at room temperature. Blocking buffer was removed from ACE2-Fc coated plates and 50 µL of RBD-HIS pre-incubated with serum was added and incubated at RT for 2 hours. Plates were washed in PBS and 0.05% Tween before 1 mg/mL anti-HIS HRP (Biolegend), diluted in PBS and 10 % FBS was added and incubated for 1 hour at RT. Plates were developed and read using conventional ELISA method.

SARS-CoV-2 production and inactivation. The New Zealand SARS-CoV-2 NZ/Queenstown/01 strain, originally isolated from a COVID-19 patient [78], was grown in VeroE6/TMPRSS2 cells (Japanese Collection of Research Bioresources Cell Bank, Osaka, Japan)[79] using DMEM (Gibco Thermo Fisher Scientific, Waltham, MA) in the absence of FBS but

supplemented with 100 units/mL of penicillin, 100 µg/mL of streptomycin, and 1 µg/mL of Geneticin™ (Gibco Thermo Fisher Scientific), and cultivated in a humidified incubator with 5% CO_2 at 37°C for 72 hours. Cell culture supernatant was harvested, clarified by centrifugation at 500 x g for 10 minutes, and stored at -80ºC. Serial 10-fold dilutions of virus were used to infect VeroE6/TMPRSS2 cells and viral replication quantified by determining cytopathic effect (CPE) and measuring cell protection using the Pierce™ BCA Protein Assay Kit (Thermo Fisher Scientific). Tissue culture dose for 50% infectivity ($TCID_{50}$) was determined in triplicate using the Reed and Muench method [75] and viral titers expressed as infectious units per milliliter (IU/mL). Approximately 30 mL of SARS-CoV-2 NZ/Queenstown/01 strain stock was thawed and filtered through a 0.45 µm steriflip filter (Merck Millipore, Burlington, MA), then inactivated with 1% formaldehyde (Sigma-Aldrich Merck, Darmstadt, Germany) for 2 hours, followed by purification using sucrose cushion ultracentrifugation (100,000 x g) for 2 hours. The purified virus was resuspended in HEPES (N-2-hydroxyethylpiperazine-N-2-ethane sulfonic acid, Thermo Fisher Scientific)-buffered saline, aliquoted, and stored at -80ºC until further use. The formaldehyde-inactivated New Zealand SARS-CoV-2 NZ/Queenstown/01 strain was quantified using NanoDrop Protein Quantification (Thermo Fisher Scientific), the Pierce™ BCA Protein Assay Kit (Thermo Fisher Scientific), and a quantitative SARS–CoV-2 RT-qPCR assay [80] (Supp. Fig. 3). An aliquot of the formaldehyde-inactivated New Zealand SARS-CoV-2 NZ/Queenstown/01 strain was tested for residual infectivity by virus titration using CPE and plaque assay after 2 72-hour serial passages in VeroE6/TMPRSS2 cells. Infection with replication-competent SARS-CoV-2 NZ/Queenstown/01 and uninfected VeroE6/TMPRSS2 cells were used as positive and negative controls, respectively (Supp. Fig. 3).

SARS-CoV-2 plaque assay. SARS-CoV-2 replication was quantified using a virus plaque assay as described [78]. Briefly, VeroE6/TMPRSS2 cells (10^6 cells/well) were seeded in 6-well plates overnight, then exposed to serial 10-fold dilutions of authentic (replication-competent) or formaldehyde-inactivated SARS-CoV-2 in infection media (DMEM with 2 % FBS, Thermo Fisher Scientific) for 1 hour. A mixture of warm overlay media (2% PBS, 63% DMEM and 35% LMP agarose, 2 mL/well) was added and the plates incubated at 37°C, 5% CO_2 for 72 hours. Agarose plugs were removed and plaques fixed with 0.5% crystal violet in 80% methanol for 20 minutes to determine viral titers expressed as plaque-forming units per milliliter (PFU/mL).

Replication-competent SARS-CoV-2 neutralization assay. The neutralization activity of serum samples collected from immunized mice or COVID-19 convalescent patients, as well as a SARS-CoV-2 spike neutralizing antibody (rabbit mAb Clone 004, SinoBiological, Beijing, China) and soluble angiotensin-converting enzyme 2 (sACE2, made in house) as controls, was assessed using a replication-competent SARS-CoV-2 isolate. Briefly, serum samples collected from immunized mice or COVID-19 convalescent patients were heat-treated at 56°C for 30 minutes, diluted with cell culture medium (1:10, then 1:5 serial dilutions), mixed with a suspension of the SARS-CoV-2 NZ/Queenstown/01 strain (0.02 multiplicity of infection) in 96-well plates at a 1:1 ratio and incubated at 37°C, 5 % CO_2 for 1 hour. The mixture was used to infect VeroE6/TMPRSS2 cells and incubated at 37°C, 5 % CO_2 for 72 hours. SARS-CoV-2 replication was quantified by determining CPE in each well and using a cell protection assay based on the Pierce™ BCA Protein Assay Kit (ThermoFisher Scientific). Neutralizing antibody titers were calculated by a non-linear regression model (log inhibitor vs. normalized response-variable slope) analysis and expressed as 50 % neutralizing titer (NT_{50}).

Generation of SARS-CoV-2 spike pseudotyped lentiviruses. Pseudotyped lentiviral particles, incorporating the spike glycoprotein from SARS-CoV-2 with 19 amino acids removed from the carboxy terminal, were generated as described by Crawford et al [81]. Briefly, HEK293T cells were seeded in 6-well plates (4 x 10^5 cells/well, in 3 mL of DMEM, 10 % FBS, 100 units/mL of penicillin, and 100 µg/mL of streptomycin, Thermo Fisher Scientific) and incubated at 37ºC, 5 % CO_2 for 24 hours. Cells were then co-transfected, using FuGENE® HD Transfection Reagent (Promega, Madison, Wisconsin), with the following plasmids: (i) 1 mg of pHAGE-CMV-Luc2-IRES-ZsGreen-W, (ii) 0.22 mg of HDM-Hgpm2, (iii) 0.22 mg of pRC-CMV-Rev1b, (iv) 0.22 mg of HDM-tat1b, and (v) 0.37 mg of a plasmid containing a codon optimized SARS-CoV-2 spike protein. In addition to the plasmid expressing the spike protein from the original ancestral isolate [82] (pcDNA3.1_spike_del19, a gift from R. De Francesco, plasmid# 155297, Addgene, Watertown, MA), a series of plasmids were synthesized to generate a comprehensive panel of pseudotyped viral particles containing codon optimized versions of the spike glycoprotein from ancestral (Wuhan), B.1.351 (Beta), P.1 (Gamma), B.1.617.2 (Delta), and B.1.1.529 (Omicron BA.1) SARS-CoV-2 variants, as well as SARS-CoV, using a pcDNA3.1 backbone (Gene Universal, Newark, DE). Cell culture media was changed 24 hours after transfection and cell-free supernatant collected 48 hours post-transfection, filtered through a 0.45 µm cellulose acetate filter (Ahlstrom Munksjo, Helsinki, Finland) and one mL aliquots stored at -80ºC until further use. The titer of the SARS-CoV-2 spike pseudotyped lentiviruses was determined by infecting HEK293 cells stably expressing human ACE2 (HEK293/ACE2 cells, obtained from Dr. John Taylor, University of Auckland) and $TCID_{50}$ values determined as described above.

*Pseudotyped virus neutralization assay***.** The ability of mouse or human serum samples to neutralize SARS-CoV-2 (or SARS-CoV)-spike-mediated entry was determined as described by Crawford et al [81]. Briefly, HEK293/ACE2 cells were seeded in poly-D-lysine coated, white-walled, 96-well plates (20,000 cells/well) and incubated at 37ºC, 5 % CO_2 for 24 hours. Serum samples collected from immunized mice or COVID-19 convalescent patients were heat-treated at 56ºC for 30 minutes, diluted with cell culture medium (1:10, then 1:5 serial dilutions), mixed with a suspension of the SARS-CoV-2 spike pseudotyped lentiviral particles (enough to generate >1,000-fold signal over background, approximately 3 to 4 x 10^5 relative light units [RLU]/well) in 96-well plates at a 1:1 ratio (150 µl final volume) and incubated at 37ºC, 5 % CO_2 for 1 hour. The cell culture media of the HEK293/ACE2 cells was removed, replaced with the mixture of serially diluted serum with SARS-CoV-2 (or SARS-CoV) spike pseudotyped lentiviruses, plus 5 µg/ml of polybrene (Sigma-Aldrich Merck), and incubated at 37ºC, 5 % CO_2 for 72 hours. Viral entry was quantified by removing the cell culture supernatant and adding a 1:1 mixture of fresh cell culture media (50 µL) and luciferin reagent (50 µL, Steady-Luc Firefly assay kit, Biotium, Fremont, CA) to each well. Plates were incubated at RT with gentle shaking (300 rpm) for 5 minutes and luminescence measured using a plate reader (VICTOR Nivo, PerkinElmer, Waltham, MA). Neutralizing antibody titers were calculated by a non-linear regression model (log inhibitor vs. normalized response-variable slope) analysis and expressed as 50 % neutralizing titer (NT_{50}).

Quantification and Statistical Analysis. Statistical analyses were performed using GraphPad Prism v.8 on pooled data from 2-4 independent experiments each with 5-10 mice per group. For immunogenicity experiments, the statistical difference between more than 2 groups was determined using a one-way ANOVA, with no matching, followed by a Tukey's post-test. The statistical difference between more than 1 variant for more than 2 groups was determined using a

two-way ANOVA. For SARS-CoV-2 challenge analysis, statistical difference was determined between the unvaccinated group compared to each other group using a Mantel-Cox Log Rank test for Survival analysis and a Mixed-effect analysis for weight loss measurements. P values of <0.05 were considered statistically significant. Figures were generated in Adobe Illustrator and BioRender.com.

Key Resources Table

Table 1: Antibodies

Item	Source	Identifier (catalog #)
Fluorescent reagents		
IgD BUV395 (clone 11-26c.2a)	BD Biosciences	564274
PD1 BUV615 (clone RMP-1)	BD Biosciences	752354
CD95 BUV805 (clone Jo2)	BD Biosciences	741968
CD38 BV421 (clone 90)	BioLegend	102732
GL7 eFluor450 (clone GL7)	Invitrogen	48-5902-80
B220 BV570 (clone RA3-6B2)	BioLegend	103237
TCRβ BV605 (clone H57-597)	BioLengend	109241
CD19 AF488 (clone 1D3)	BioLegend	115521
CD138 BB700 (clone 281-2)	BD Biosciences	142526
IRF4 PerCP eFluor 710 (clone 3E4)	Invitrogen	46-9858-82
Zombie NIR fixable viability kit	BioLegend	423105
SAV BV711	BD Biosciences	563262
SAV PE	BioLegend	405204
CD4 BV510 (clone GK1.5)	BioLegend	100449
CD44 AF700 (clone IM7)	BD Biosciences	560567
PD-1 PE Cy7 (clone 29F.1A12)	BioLegend	135216
Bcl6 AF647 (clone K112-91)	BD Biosciences	561525
ELISA, protein isolation and ELISpot reagents		
Mouse anti-human IgG (Fc) HRP	BioRad	MCA647P
Goat anti-mouse total IgG HRP	Invitrogen	G21040
ELISpot Plus: Mouse IFN-γ (ALP)	Mabtech	3321-4AST-10
anti-FLAG® M2 affinity resin	Sigma	F3165-5MG
Monoclonal mouse anti-spike IgG1 clone 43 antibody	SinoBiological	40591-MM43
anti-spike IgG1 Clone 43 antibody	SinoBiological	40591-MM43
anti-HIS tag HRP	Biolegends	J099B12

Table 2: Labware

Item	Source	Identifier (catalog #)
1mL syringe	BD Biosciences	302113
3mL syringe	BD Biosciences	302100
PCR plates	BioRad	HSS9601
70µM cell strainer	Falcon	BDAA352350
Microvette serum gel tubes	Sarstedt	SARS20.1344
Nunc MaxiSorp™ 96-Well ELISA microplates	ThermoFisher	442404
optical-quality sealing tape	BioRad	2239444
S-Microvette® serum gel tubes	Sarstedt	20.1344

Table 3: Reagents

Item	Source	Identifier catalog
HEK293 GnTI-	American Type Culture Collection ATCC, Manassas, VA	CRL-3022
VeroE6/TMPRSS2 cells	Japanese Collection of Research Bioresources Cell Bank, Osaka, Japan	JCRB No: JCRB1819
Bellocell	Cesco Bioengineering, Taiwan	BelloCell-500
Fetal bovine serum	Gibco Thermo Fisher Scientific	10091-148
DMEM	Gibco Thermo Fisher Scientific	12491015
fetal bovine serum	Gibco Thermo Fisher Scientific	A4766801
Iscove's Modified Dulbecco's Medium (IMDM)	Gibco Thermo Fisher Scientific	31980097
streptomycin, and 1 µg/ml of Geneticin™	Gibco Thermo Fisher Scientific	10131035
IMDM, GlutaMAX™ supplement	Gibco Thermo Fisher Scientific	31980-097
RPMI 1640 medium	Gibco Thermo Fisher Scientific	11875-119
FuGENE® HD Transfection Reagent	Promega	E2311
polybrene	Sigma-Aldrich Merck,	S4400
100 units/ml of penicillin, and 100 µg/ml of streptomycin,	Thermo Fisher Scientific	15140122
HEPES (N-2-hydroxyethylpiperazine-N-2-ethane sulfonic acid)	Thermo Fisher Scientific-	7365-45-9
OptEIA™ TMB substrate reagent set	BD OptEIA™	51-2606KC and 51-2607KC
Step Ultra TMB-ELISA HRP substrate	Thermo Scientific™	34028
NotI	New England Biolabs	R0189L
XbaI	New England Biolabs	R0145T

HRV-3C protease (LEVLFQ/GP)		
Protein A-CaptivATM PriMAB	RepliGen	CA-PRI-0005

Item	Source	Identifier
eBioscience™ FoxP3/transcription factor fixation/permeabilisation kit	Invitrogen	00-5521-00
Red blood cell lysis solution	Qiagen	158904
Biotin powder	Sigma-Aldrich	B4501-1G
AddaVax™	Invivogen	vac-adx-10
PepMix™ SARS-CoV-2 (spike glycoprotein)	JPT	PM-WCPV-S-1
PepMix™ SARS-CoV-2 (S-RBD B.1.617.2 / Delta)	JPT	PM-SARS2-RBDMUT06-1
PepMix™ SARS-CoV-2 (Spike B.1.617.2 / Delta)	JPT	PM-SARS2-SMUT06-1
OptEIA™ TMB substrate reagent set	BD Biosciences	555214
0.45 µm steriflip filter	Merck Millipore	32031602
Tween	Sigma Aldrich	P9416
Urea powder	Sigma-Aldrich	U5378-500G
formaldehyde	Sigma-Aldrich Merck, Darmstadt, Germany	47608
non-fat dry milk	Alpine	
HiTrap MabSelect PrismA – GSTrap™ HP	Cytiva	28-4082-53
Superose 6 Increase 10/300 GL	Cytiva	17-5172-01
400x SYPRO Orange	Sigma	O3756-100G
HiLoad 16/600 Superdex 200 PG column	Sigma Aldrich	GE28-9893-35
Pierce™ BCA Protein Assay Kit	Thermo Fisher Scientific,	23227
Fc Block 2.4G2	Made in house	
hACE	Made in house	
Beta RBD-his	Sino biological	40592-V08H59
Omicron RBD-his	Sino biological	40592-V08H121
Omicron S1-his	Sino biological	40591-V08H41

References

1. Landsberg, H.E., Turcinovic, J., Sullivan, M., Connor, J.H., Hamer, D.H., and Platt, J.T. (2022). Efficacy of Pfizer-BioNTech in SARS-CoV-2 Delta cluster. Int J Infect Dis *114*, 62-64. 10.1016/j.ijid.2021.10.053.
2. Francis, A.I., Ghany, S., Gilkes, T., and Umakanthan, S. (2021). Review of COVID-19 vaccine subtypes, efficacy and geographical distributions. Postgrad Med J. 10.1136/postgradmedj-2021-140654.
3. Carnell, G.W., Ciazynska, K.A., Wells, D.A., Xiong, X., Aguinam, E.T., McLaughlin, S.H., Mallery, D., Ebrahimi, S., Ceron-Gutierrez, L., James, L.C., et al. SARS-CoV-2 spike protein arrested in the closed state induces potent neutralizing responses. BioRxiv. 10.1101/2021.01.14.426695.
4. Ou, X., Liu, Y., Lei, X., Li, P., Mi, D., Ren, L., Guo, L., Guo, R., Chen, T., Hu, J., et al. (2020). Characterization of spike glycoprotein of SARS-CoV-2 on virus entry and its immune cross-reactivity with SARS-CoV. Nature communications *11*, 1620-1620. 10.1038/s41467-020-15562-9.
5. Starr, T.N., Greaney, A.J., Hilton, S.K., Ellis, D., Crawford, K.H.D., Dingens, A.S., Navarro, M.J., Bowen, J.E., Tortorici, M.A., Walls, A.C., et al. (2020). Deep Mutational Scanning of SARS-CoV-2 Receptor Binding Domain Reveals Constraints on Folding and ACE2 Binding. Cell *182*, 1295-1310 e1220. 10.1016/j.cell.2020.08.012.
6. Martinez-Flores, D., Zepeda-Cervantes, J., Cruz-Resendiz, A., Aguirre-Sampieri, S., Sampieri, A., and Vaca, L. (2021). SARS-CoV-2 Vaccines Based on the Spike Glycoprotein and Implications of New Viral Variants. Front Immunol *12*, 701501. 10.3389/fimmu.2021.701501.
7. Walls, A.C., Park, Y.J., Tortorici, M.A., Wall, A., McGuire, A.T., and Veesler, D. (2020). Structure, Function, and Antigenicity of the SARS-CoV-2 Spike Glycoprotein. Cell *181*, 281-292.e286. 10.1016/j.cell.2020.02.058.
8. Barnes, C.O., West, A.P., Jr., Huey-Tubman, K.E., Hoffmann, M.A.G., Sharaf, N.G., Hoffman, P.R., Koranda, N., Gristick, H.B., Gaebler, C., Muecksch, F., et al. (2020). Structures of Human Antibodies Bound to SARS-CoV-2 Spike Reveal Common Epitopes and Recurrent Features of Antibodies. Cell *182*, 828-842 e816. 10.1016/j.cell.2020.06.025.
9. Vangelista, L., and Secchi, M. (2020). Prepare for the Future: Dissecting the Spike to Seek Broadly Neutralizing Antibodies and Universal Vaccine for Pandemic Coronaviruses. Frontiers in Molecular Biosciences *7*. 10.3389/fmolb.2020.00226.
10. Cao, Y., Su, B., Guo, X., Sun, W., Deng, Y., Bao, L., Zhu, Q., Zhang, X., Zheng, Y., Geng, C., et al. (2020). Potent neutralizing antibodies against SARS-CoV-2 identified by high-throughput single-cell sequencing of convalescent patients' B cells. Cell. 10.1016/j.cell.2020.05.025.
11. Chi, X., Yan, R., Zhang, J., Zhang, G., Zhang, Y., Hao, M., Zhang, Z., Fan, P., Dong, Y., Yang, Y., et al. (2020). A neutralizing human antibody binds to the N-terminal domain of the Spike protein of SARS-CoV-2. Science *369*, 650-655. 10.1126/science.abc6952.
12. McCallum, M., De Marco, A., Lempp, F.A., Tortorici, M.A., Pinto, D., Walls, A.C., Beltramello, M., Chen, A., Liu, Z., Zatta, F., et al. (2021). N-terminal domain antigenic mapping reveals a site of vulnerability for SARS-CoV-2. Cell *184*, 2332-2347 e2316. 10.1016/j.cell.2021.03.028.
13. Yang, J., Wang, W., Chen, Z., Lu, S., Yang, F., Bi, Z., Bao, L., Mo, F., Li, X., Huang, Y., et al. (2020). A vaccine targeting the RBD of the S protein of SARS-CoV-2 induces protective immunity. Nature *586*, 572-577. 10.1038/s41586-020-2599-8.
14. Yu, F., Xiang, R., Deng, X., Wang, L., Yu, Z., Tian, S., Liang, R., Li, Y., Ying, T., and Jiang, S. (2020). Receptor-binding domain-specific human neutralizing monoclonal antibodies against SARS-CoV

and SARS-CoV-2. Signal Transduction and Targeted Therapy *5*, 1-12. 10.1038/s41392-020-00318-0.

15. Yuan, M., Wu, N.C., Zhu, X., Lee, C.C.D., So, R.T.Y., Lv, H., Mok, C.K.P., and Wilson, I.A. (2020). A highly conserved cryptic epitope in the receptor binding domains of SARS-CoV-2 and SARS-CoV. Science (New York, N.Y.) *368*, 630-633. 10.1126/science.abb7269.
16. Amanat, F., Thapa, M., Lei, T., Ahmed, S.M.S., Adelsberg, D.C., Carreno, J.M., Strohmeier, S., Schmitz, A.J., Zafar, S., Zhou, J.Q., et al. (2021). SARS-CoV-2 mRNA vaccination induces functionally diverse antibodies to NTD, RBD, and S2. Cell *184*, 3936-3948 e3910. 10.1016/j.cell.2021.06.005.
17. Li, L., Zhao, Z., Yang, X., Li, W., Chen, S., Sun, T., Wang, L., He, Y., Liu, G., Han, X., et al. (2020). Identification of four linear B-cell epitopes on the SARS-CoV-2 spike protein able to elicit neutralizing antibodies. BioRxiv. 10.1101/2020.12.13.422550.
18. Li, Y., Ma, M.L., Lei, Q., Wang, F., Hong, W., Lai, D.Y., Hou, H., Xu, Z.W., Zhang, B., Chen, H., et al. (2021). Linear epitope landscape of the SARS-CoV-2 Spike protein constructed from 1,051 COVID-19 patients. Cell Rep *34*, 108915. 10.1016/j.celrep.2021.108915.
19. Ng, K.W., Faulkner, N., Cornish, G.H., Rosa, A., Harvey, R., Hussain, S., Ulferts, R., Earl, C., Wrobel, A., Benton, D., et al. (2021). Pre-existing and de novo humoral immunity to SARS-CoV-2 in humans.
20. Voss, W.N., Hou, Y.J., Johnson, N.V., Delidakis, G., Kim, J.E., Javanmardi, K., Horton, A.P., Bartzoka, F., Paresi, C.J., Tanno, Y., et al. (2021). Prevalent, protective, and convergent IgG recognition of SARS-CoV-2 non-RBD spike epitopes. Science *372*, 1108-1112. 10.1126/science.abg5268.
21. Hatzakis, A., Karabinis, A., Roussos, S., Pantazis, N., Degiannis, D., Chaidaroglou, A., Petsios, K., Pavlopoulou, I., Tsiodras, S., Paraskevis, D., et al. (2022). Modelling SARS-CoV-2 Binding Antibody Waning 8 Months after BNT162b2 Vaccination. Vaccines (Basel) *10*. 10.3390/vaccines10020285.
22. Goel, R.R., Painter, M.M., Lundgreen, K.A., Apostolidis, S.A., Baxter, A.E., Giles, J.R., Mathew, D., Pattekar, A., Reynaldi, A., Khoury, D.S., et al. (2022). Efficient recall of Omicron-reactive B cell memory after a third dose of SARS-CoV-2 mRNA vaccine. bioRxiv. 10.1101/2022.02.20.481163.
23. Wu, Y., Huang, X., Yuan, L., Wang, S., Zhang, Y., Xiong, H., Chen, R., Ma, J., Qi, R., Nie, M., et al. (2021). A recombinant spike protein subunit vaccine confers protective immunity against SARS-CoV-2 infection and transmission in hamsters. https://www.science.org.
24. Wang, Y., Wang, L., Cao, H., and Liu, C. (2021). SARS-CoV-2 S1 is superior to the RBD as a COVID-19 subunit vaccine antigen. J Med Virol *93*, 892-898. 10.1002/jmv.26320.
25. Wen, Y., Jing, Y., Yang, L., Kang, D., Jiang, P., Li, N., Cheng, J., Li, J., Li, X., Peng, Z., et al. (2019). The regulators of BCR signaling during B cell activation. Blood Science *1*, 119-129. 10.1097/bs9.0000000000000026.
26. Bachmann, M.F., and Jennings, G.T. (2010). Vaccine delivery: a matter of size, geometry, kinetics and molecular patterns. Nat Rev Immunol *10*, 787-796. 10.1038/nri2868.
27. Pan, X., Shi, J., Hu, X., Wu, Y., Zeng, L., Yao, Y., Shang, W., Liu, K., Gao, G., Guo, W., et al. (2021). RBD-homodimer, a COVID-19 subunit vaccine candidate, elicits immunogenicity and protection in rodents and nonhuman primates. Cell Discov *7*, 82. 10.1038/s41421-021-00320-y.
28. Dai, L., Zheng, T., Xu, K., Han, Y., Xu, L., Huang, E., An, Y., Cheng, Y., Li, S., Liu, M., et al. (2020). A Universal Design of Betacoronavirus Vaccines against COVID-19, MERS, and SARS. Cell *182*, 722-733 e711. 10.1016/j.cell.2020.06.035.
29. Roltgen, K., Nielsen, S.C.A., Silva, O., Younes, S.F., Zaslavsky, M., Costales, C., Yang, F., Wirz, O.F., Solis, D., Hoh, R.A., et al. (2022). Immune imprinting, breadth of variant recognition, and

germinal center response in human SARS-CoV-2 infection and vaccination. Cell *185*, 1025-1040 e1014. 10.1016/j.cell.2022.01.018.

30. Laidlaw, B.J., and Ellebedy, A.H. (2022). The germinal centre B cell response to SARS-CoV-2. Nat Rev Immunol *22*, 7-18. 10.1038/s41577-021-00657-1.
31. Sette, A., and Crotty, S. (2020). Pre-existing immunity to SARS-CoV-2: the knowns and unknowns. Nature Reviews Immunology *20*, 457-458. 10.1038/s41577-020-0389-z.
32. Tarke, A., Sidney, J., Kidd, C.K., Dan, J.M., Ramirez, S.I., Yu, E.D., Mateus, J., da Silva Antunes, R., Moore, E., Rubiro, P., et al. (2021). Comprehensive analysis of T cell immunodominance and immunoprevalence of SARS-CoV-2 epitopes in COVID-19 cases. Cell Rep Med *2*, 100204. 10.1016/j.xcrm.2021.100204.
33. Brewer, R.C., Ramadoss, N.S., Lahey, L.J., Jahanbani, S., Robinson, W.H., and Lanz, T.V. (2022). BNT162b2 vaccine induces divergent B cell responses to SARS-CoV-2 S1 and S2. Nat Immunol *23*, 33-39. 10.1038/s41590-021-01088-9.
34. Turk, L.S., Kuang, X., Dal Pozzo, V., Patel, K., Chen, M., Huynh, K., Currie, M.J., Mitchell, D., Dobson, R.C.J., D'Arcangelo, G., et al. (2021). The structure-function relationship of a signaling-competent, dimeric Reelin fragment. Structure *29*, 1156-1170 e1156. 10.1016/j.str.2021.05.012.
35. KUPFERSCHMIDT, K., and WADMAN, M. (2021). Delta variant triggers new phase in the pandemic. Science *372*, 1375-1376. 10.1126/science.372.6549.1375.
36. Zheng, J., Wong, L.R., Li, K., Verma, A.K., Ortiz, M.E., Wohlford-Lenane, C., Leidinger, M.R., Knudson, C.M., Meyerholz, D.K., McCray, P.B., Jr., and Perlman, S. (2021). COVID-19 treatments and pathogenesis including anosmia in K18-hACE2 mice. Nature *589*, 603-607. 10.1038/s41586-020-2943-z.
37. McCray, P.B., Jr., Pewe, L., Wohlford-Lenane, C., Hickey, M., Manzel, L., Shi, L., Netland, J., Jia, H.P., Halabi, C., Sigmund, C.D., et al. (2007). Lethal infection of K18-hACE2 mice infected with severe acute respiratory syndrome coronavirus. J Virol *81*, 813-821. 10.1128/JVI.02012-06.
38. Oladunni, F.S., Park, J.G., Pino, P.A., Gonzalez, O., Akhter, A., Allue-Guardia, A., Olmo-Fontanez, A., Gautam, S., Garcia-Vilanova, A., Ye, C., et al. (2020). Lethality of SARS-CoV-2 infection in K18 human angiotensin-converting enzyme 2 transgenic mice. Nat Commun *11*, 6122. 10.1038/s41467-020-19891-7.
39. Gazit, S., Shlezinger, R., Perez, G., Lotan, R., Peretz, A., Ben-Tov, A., Cohen, D., Muhsen, K., Chodick, G., and Patalon, T. (2021). Comparing SARS-CoV-2 natural immunity to vaccine-induced immunity: reinfections versus breakthrough infections

. bioRxiv : the preprint server for biology

. 10.1101/2021.08.24.21262415.

40. Gao, Q., Bao, L., Mao, H., Wang, L., Xu, K., Yang, M., Li, Y., Zhu, L., Wang, N., Lv, Z., et al. (2020). Development of an inactivated vaccine candidate for SARS-CoV-2. Science *369*, 77-81. 10.1126/science.abc1932.
41. Jara, A., Undurraga, E.A., Gonzalez, C., Paredes, F., Fontecilla, T., Jara, G., Pizarro, A., Acevedo, J., Leo, K., Leon, F., et al. (2021). Effectiveness of an Inactivated SARS-CoV-2 Vaccine in Chile. N Engl J Med *385*, 875-884. 10.1056/NEJMoa2107715.
42. Crotty, S. (2011). Follicular helper CD4 T cells (TFH). Annual review of immunology *29*, 621-663. 10.1146/annurev-immunol-031210-101400.
43. Harfoot, R., Lawley, B., Hernandez, L.C., Kuang, J., Hills, F.R., Sinha, S., Allais, M.J.M., Bird, T.W., Taylor, J.A., Bostina, M., Comoletti, D., Haney, E.F., Hancock, R.E.W., Pletzer, D., and Quiñones-Mateu, M.E ((2022)). Synthetic host defense peptide inhibits SARS-CoV-2 replication in vitro. . Under review

44. Zeng, B., Gao, L., Zhou, Q., Yu, K., and Sun, F. (2022). Effectiveness of COVID-19 vaccines against SARS-CoV-2 variants of concern: a systematic review and meta-analysis. BMC Med *20*, 200. 10.1186/s12916-022-02397-y.
45. Polack, F.P., Thomas, S.J., Kitchin, N., Absalon, J., Gurtman, A., Lockhart, S., Perez, J.L., Perez Marc, G., Moreira, E.D., Zerbini, C., et al. (2020). Safety and Efficacy of the BNT162b2 mRNA Covid-19 Vaccine. N Engl J Med *383*, 2603-2615. 10.1056/NEJMoa2034577.
46. Kato, H., Miyakawa, K., Ohtake, N., Go, H., Yamaoka, Y., Yajima, S., Shimada, T., Goto, A., Nakajima, H., and Ryo, A. (2022). Antibody titers against the Alpha, Beta, Gamma, and Delta variants of SARS-CoV-2 induced by BNT162b2 vaccination measured using automated chemiluminescent enzyme immunoassay. J Infect Chemother *28*, 273-278. 10.1016/j.jiac.2021.11.021.
47. Sahin, U., Muik, A., Vogler, I., Derhovanessian, E., Kranz, L.M., Vormehr, M., Quandt, J., Bidmon, N., Ulges, A., Baum, A., et al. (2021). BNT162b2 vaccine induces neutralizing antibodies and poly-specific T cells in humans. Nature *595*, 572-577. 10.1038/s41586-021-03653-6.
48. Muik, A., Lui, B.G., Wallisch, A.K., Bacher, M., Muhl, J., Reinholz, J., Ozhelvaci, O., Beckmann, N., Guimil Garcia, R.C., Poran, A., et al. (2022). Neutralization of SARS-CoV-2 Omicron by BNT162b2 mRNA vaccine-elicited human sera. Science *375*, 678-680. 10.1126/science.abn7591.
49. Ai, J., Zhang, H., Zhang, Y., Lin, K., Zhang, Y., Wu, J., Wan, Y., Huang, Y., Song, J., Fu, Z., et al. (2022). Omicron variant showed lower neutralizing sensitivity than other SARS-CoV-2 variants to immune sera elicited by vaccines after boost. Emerg Microbes Infect *11*, 337-343. 10.1080/22221751.2021.2022440.
50. Eisen, H.N. (2014). Affinity Enhancement of Antibodies: How Low-Affinity Antibodies Produced Early in Immune Responses Are Followed by High-Affinity Antibodies Later and in Memory B-Cell Responses. Cancer Immunology Research *2*, 381-392. 10.1158/2326-6066.CIR-14-0029.
51. Kleanthous, H., Silverman, J.M., Makar, K.W., Yoon, I.K., Jackson, N., and Vaughn, D.W. (2021). Scientific rationale for developing potent RBD-based vaccines targeting COVID-19. NPJ Vaccines *6*, 128. 10.1038/s41541-021-00393-6.
52. Fierz, W., and Walz, B. (2020). Antibody Dependent Enhancement Due to Original Antigenic Sin and the Development of SARS. Front Immunol *11*, 1120. 10.3389/fimmu.2020.01120.
53. Lee, W.S., Wheatley, A.K., Kent, S.J., and DeKosky, B.J. (2020). Antibody-dependent enhancement and SARS-CoV-2 vaccines and therapies. Nat Microbiol *5*, 1185-1191. 10.1038/s41564-020-00789-5.
54. Yip, M.S., Leung, H.L., Li, P.H., Cheung, C.Y., Dutry, I., Li, D., Daeron, M., Bruzzone, R., Peiris, J.S., and Jaume, M. (2016). Antibody-dependent enhancement of SARS coronavirus infection and its role in the pathogenesis of SARS. Hong Kong Med J *22*, 25-31.
55. Yip, M.S., Leung, N.H., Cheung, C.Y., Li, P.H., Lee, H.H., Daeron, M., Peiris, J.S., Bruzzone, R., and Jaume, M. (2014). Antibody-dependent infection of human macrophages by severe acute respiratory syndrome coronavirus. Virol J *11*, 82. 10.1186/1743-422X-11-82.
56. Wang, S.F., Tseng, S.P., Yen, C.H., Yang, J.Y., Tsao, C.H., Shen, C.W., Chen, K.H., Liu, F.T., Liu, W.T., Chen, Y.M., and Huang, J.C. (2014). Antibody-dependent SARS coronavirus infection is mediated by antibodies against spike proteins. Biochem Biophys Res Commun *451*, 208-214. 10.1016/j.bbrc.2014.07.090.
57. Tracker, V.G.C.V. (2022). COVID19 Vaccine Tracker.
58. Choe, P.G., Kang, C.K., Suh, H.J., Jung, J., Song, K.H., Bang, J.H., Kim, E.S., Kim, H.B., Park, S.W., Kim, N.J., et al. (2021). Waning Antibody Responses in Asymptomatic and Symptomatic SARS-CoV-2 Infection. Emerg Infect Dis *27*. 10.3201/eid2701.203515.

59. Levin, E.G., Lustig, Y., Cohen, C., Fluss, R., Indenbaum, V., Amit, S., Doolman, R., Asraf, K., Mendelson, E., Ziv, A., et al. (2021). Waning Immune Humoral Response to BNT162b2 Covid-19 Vaccine over 6 Months. N Engl J Med *385*, e84. 10.1056/NEJMoa2114583.
60. Bartleson, J.M., Radenkovic, D., Covarrubias, A.J., Furman, D., Winer, D.A., and Verdin, E. (2021). SARS-CoV-2, COVID-19 and the Ageing Immune System. Nat Aging *1*, 769-782. 10.1038/s43587-021-00114-7.
61. Zhao, J., Zhao, J., Mangalam, A.K., Channappanavar, R., Fett, C., Meyerholz, D.K., Agnihothram, S., Baric, R.S., David, C.S., and Perlman, S. (2016). Airway Memory CD4(+) T Cells Mediate Protective Immunity against Emerging Respiratory Coronaviruses. Immunity *44*, 1379-1391. 10.1016/j.immuni.2016.05.006.
62. Minervina, A.A., Komech, E.A., Titov, A., Bensouda Koraichi, M., Rosati, E., Mamedov, I.Z., Franke, A., Efimov, G.A., Chudakov, D.M., Mora, T., et al. (2021). Longitudinal high-throughput TCR repertoire profiling reveals the dynamics of T-cell memory formation after mild COVID-19 infection. Elife *10*. 10.7554/eLife.63502.
63. Schultheiß, C., Paschold, L., Simnica, D., Mohme, M., Willscher, E., Wenserski, L.v., Scholz, R., Wieters, I., Dahlke, C., Tolosa, E., et al. (2020). Next Generation Sequencing of T and B cell receptor repertoires from COVID-19 patients showed signatures associated with severity of disease. Immunity *0*, 1-14. 10.1016/j.immuni.2020.06.024.
64. Grifoni, A., Weiskopf, D., Ramirez, S.I., Mateus, J., Dan, J.M., Moderbacher, C.R., Rawlings, S.A., Sutherland, A., Premkumar, L., Jadi, R.S., et al. (2020). Targets of T Cell Responses to SARS-CoV-2 Coronavirus in Humans with COVID-19 Disease and Unexposed Individuals. Cell *181*, 1489-1501.e1415. 10.1016/j.cell.2020.05.015.
65. Kent, S.J., Khoury, D.S., Reynaldi, A., Juno, J.A., Wheatley, A.K., Stadler, E., John Wherry, E., Triccas, J., Sasson, S.C., Cromer, D., and Davenport, M.P. (2022). Disentangling the relative importance of T cell responses in COVID-19: leading actors or supporting cast? Nat Rev Immunol *22*, 387-397. 10.1038/s41577-022-00716-1.
66. Israelow, B., Mao, T., Klein, J., Song, E., Menasche, B., Omer, S.B., and Iwasaki, A. (2021). Adaptive immune determinants of viral clearance and protection in mouse models of SARS-CoV-2. Sci Immunol *6*, eabl4509. 10.1126/sciimmunol.abl4509.
67. Chia, W.N., Zhu, F., Ong, S.W.X., Young, B.E., Fong, S.-W., Le Bert, N., Tan, C.W., Tiu, C., Zhang, J., Tan, S.Y., et al. (2021). Dynamics of SARS-CoV-2 neutralising antibody responses and duration of immunity: a longitudinal study. The Lancet Microbe *2*, e240-e249. 10.1016/s2666-5247(21)00025-2.
68. Perez-Alos, L., Armenteros, J.J.A., Madsen, J.R., Hansen, C.B., Jarlhelt, I., Hamm, S.R., Heftdal, L.D., Pries-Heje, M.M., Moller, D.L., Fogh, K., et al. (2022). Modeling of waning immunity after SARS-CoV-2 vaccination and influencing factors. Nat Commun *13*, 1614. 10.1038/s41467-022-29225-4.
69. Liu, J., Chandrashekar, A., Sellers, D., Barrett, J., Jacob-Dolan, C., Lifton, M., McMahan, K., Sciacca, M., VanWyk, H., Wu, C., et al. (2022). Vaccines elicit highly conserved cellular immunity to SARS-CoV-2 Omicron. Nature *603*, 493-496. 10.1038/s41586-022-04465-y.
70. Greaney, A.J., Loes, A.N., Gentles, L.E., Crawford, K.H.D., Starr, T.N., Malone, K.D., Chu, H.Y., and Bloom, J.D. (2021). Antibodies elicited by mRNA-1273 vaccination bind more broadly to the receptor binding domain than do those from SARS-CoV-2 infection. Sci Transl Med *13*. 10.1126/scitranslmed.abi9915.
71. Ranaivoson, F.M., Turk, L.S., Ozgul, S., Kakehi, S., von Daake, S., Lopez, N., Trobiani, L., De Jaco, A., Denissova, N., Demeler, B., et al. (2019). A Proteomic Screen of Neuronal Cell-Surface Molecules Reveals IgLONs as Structurally Conserved Interaction Modules at the Synapse. Structure *27*, 893-906 e899. 10.1016/j.str.2019.03.004.

72. Rubio-Marrero, E.N., Vincelli, G., Jeffries, C.M., Shaikh, T.R., Pakos, I.S., Ranaivoson, F.M., von Daake, S., Demeler, B., De Jaco, A., Perkins, G., et al. (2016). Structural Characterization of the Extracellular Domain of CASPR2 and Insights into Its Association with the Novel Ligand Contactin1. J Biol Chem *291*, 5788-5802. 10.1074/jbc.M115.705681.
73. Chen, W.H., Pollet, J., Strych, U., Lee, J., Liu, Z., Kundu, R.T., Versteeg, L., Villar, M.J., Adhikari, R., Wei, J., et al. (2022). Yeast-expressed recombinant SARS-CoV-2 receptor binding domain RBD203-N1 as a COVID-19 protein vaccine candidate. Protein Expr Purif *190*, 106003. 10.1016/j.pep.2021.106003.
74. Liu, W.W., Zhu, Y., and Fang, Q. (2017). Femtomole-Scale High-Throughput Screening of Protein Ligands with Droplet-Based Thermal Shift Assay. Anal Chem *89*, 6678-6685. 10.1021/acs.analchem.7b00899.
75. Reed, L.J., and Muench, H. (1938). A simple method of estimating fifty percent endpoints. Am.J.Hyg *27* 493-497.
76. Ramakrishnan, M.A. (2016). Determination of 50% endpoint titer using a simple formula. World J Virol *5*, 85-86. 10.5501/wjv.v5.i2.85.
77. Frey, A., Di Canzio, J., and Zurakowski, D. (1998). A statistically defined endpoint titer determination method for immunoassays. J Immunol Methods *221*, 35-41. 10.1016/s0022-1759(98)00170-7.
78. Harfoot, R., Lawley, B., Hernandez, L.C., Kuang, J., Grant, J., Treece, J.M., Lequeux, S., Day, R., Stanton, J.-A.L., Bostina, M., et al. (2022). First Isolation and Characterization of SARS-CoV-2 in Aotearoa New Zealand as Part of a Rapid response to the COVID-19 Pandemic in Early 2020. Viruses.
79. Yamada, S., Fukushi, S., Kinoshita, H., Ohnishi, M., Suzuki, T., Fujimoto, T., Saijo, M., and Maeda, K. (2021). Assessment of SARS-CoV-2 infectivity of upper respiratory specimens from COVID-19 patients by virus isolation using VeroE6/TMPRSS2 cells. BMJ Open Respir Res *8*. 10.1136/bmjresp-2020-000830.
80. Lawley, B., Grant, J., Harfoot, R., Treece, J.M., Day, R., Hernandez, L.C., Stanton, J.L., Ussher, J.E., and Quinones-Mateu, M.E. (2021). Rapid Response to SARS-CoV-2 in Aotearoa New Zealand: Implementation of a Diagnostic Test and Characterization of the First COVID-19 Cases in the South Island. Viruses *13*. 10.3390/v13112222.
81. Crawford, K.H.D., Eguia, R., Dingens, A.S., Loes, A.N., Malone, K.D., Wolf, C.R., Chu, H.Y., Tortorici, M.A., Veesler, D., Murphy, M., et al. (2020). Protocol and Reagents for Pseudotyping Lentiviral Particles with SARS-CoV-2 Spike Protein for Neutralization Assays. Viruses *12*. 10.3390/v12050513.
82. Zhu, N., Zhang, D., Wang, W., Li, X., Yang, B., Song, J., Zhao, X., Huang, B., Shi, W., Lu, R., et al. (2020). A Novel Coronavirus from Patients with Pneumonia in China, 2019. N Engl J Med *382*, 727-733. 10.1056/NEJMoa2001017.

A

B

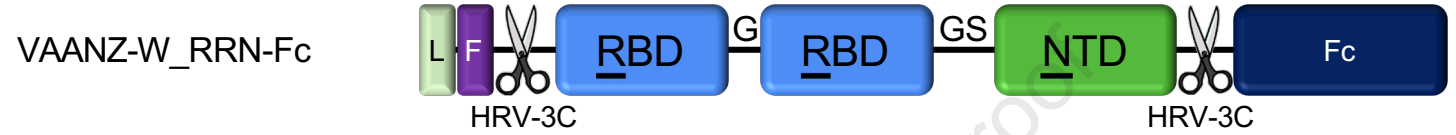

C

Name	Domain architecture	Variant	Length – MW (kDa)
W_RBD	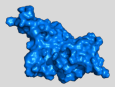	Ancestral, Wuhan	218 – 24.4
W_RBD-RBD	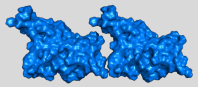	Ancestral, Wuhan	455 – 50.8
Δ_RBD-RBD	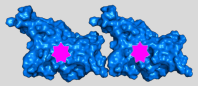	Delta, B.1.617.2 L452R, T478K	455 – 50.8
W_NTD-RBD	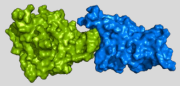	Ancestral, Wuhan	500 – 56.3
VAANZ-W_RRN	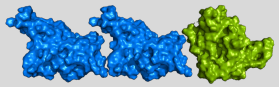	Ancestral, Wuhan	716 – 81.4
VAANZ-Δ_RRN	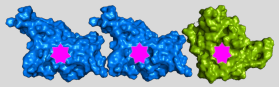	Delta, B.1.617.2 L452R, T478K (RBD); T19R, G142D, 156-157del, R158G (NTD)	726 – 81.9

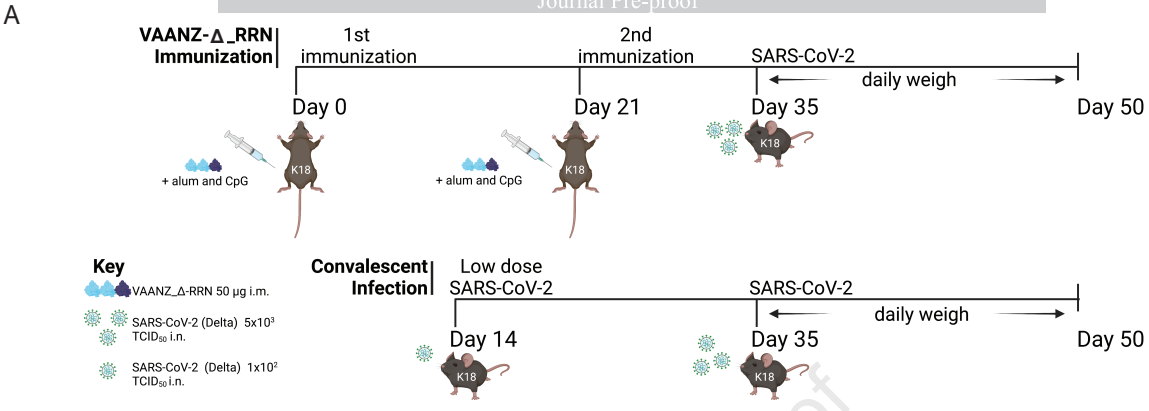

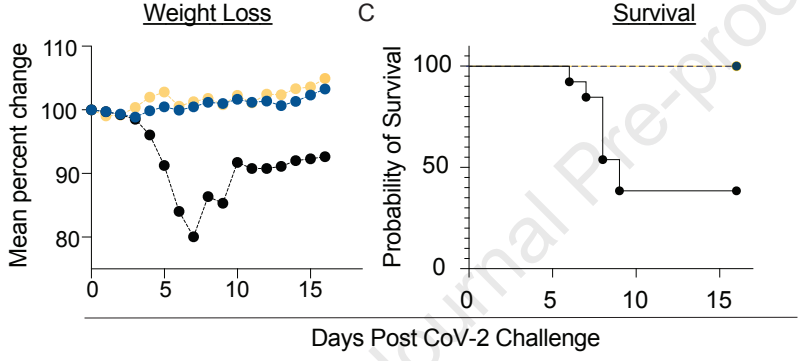

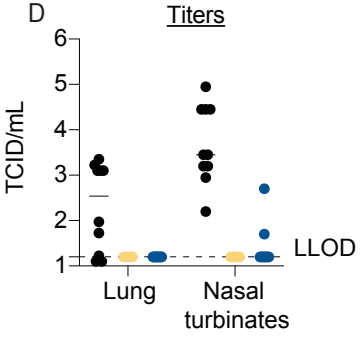

	Significant to unvaccinated			Viral titer	
	Weight loss	Survival	No. mice alive	Lung	Nasal
Unvaccinated			5/13		
Convalescent	****	****	10/10	****	****
VAANZ_Δ-RRN	****	****	10/10	****	****

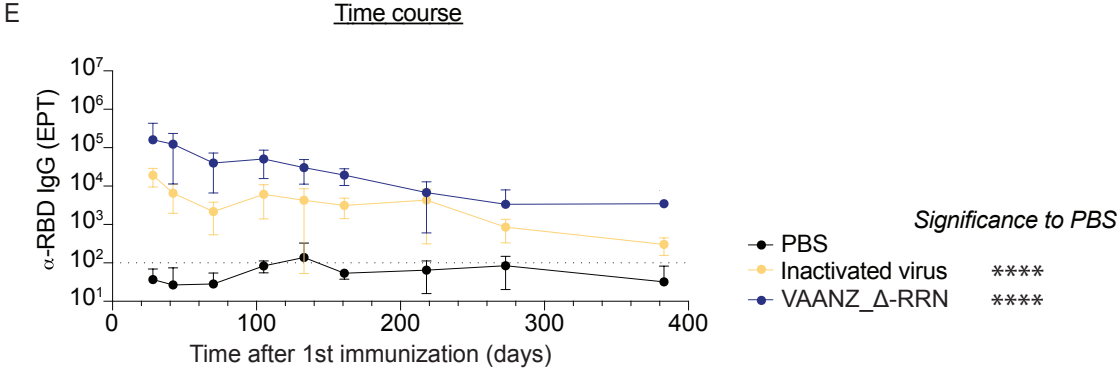

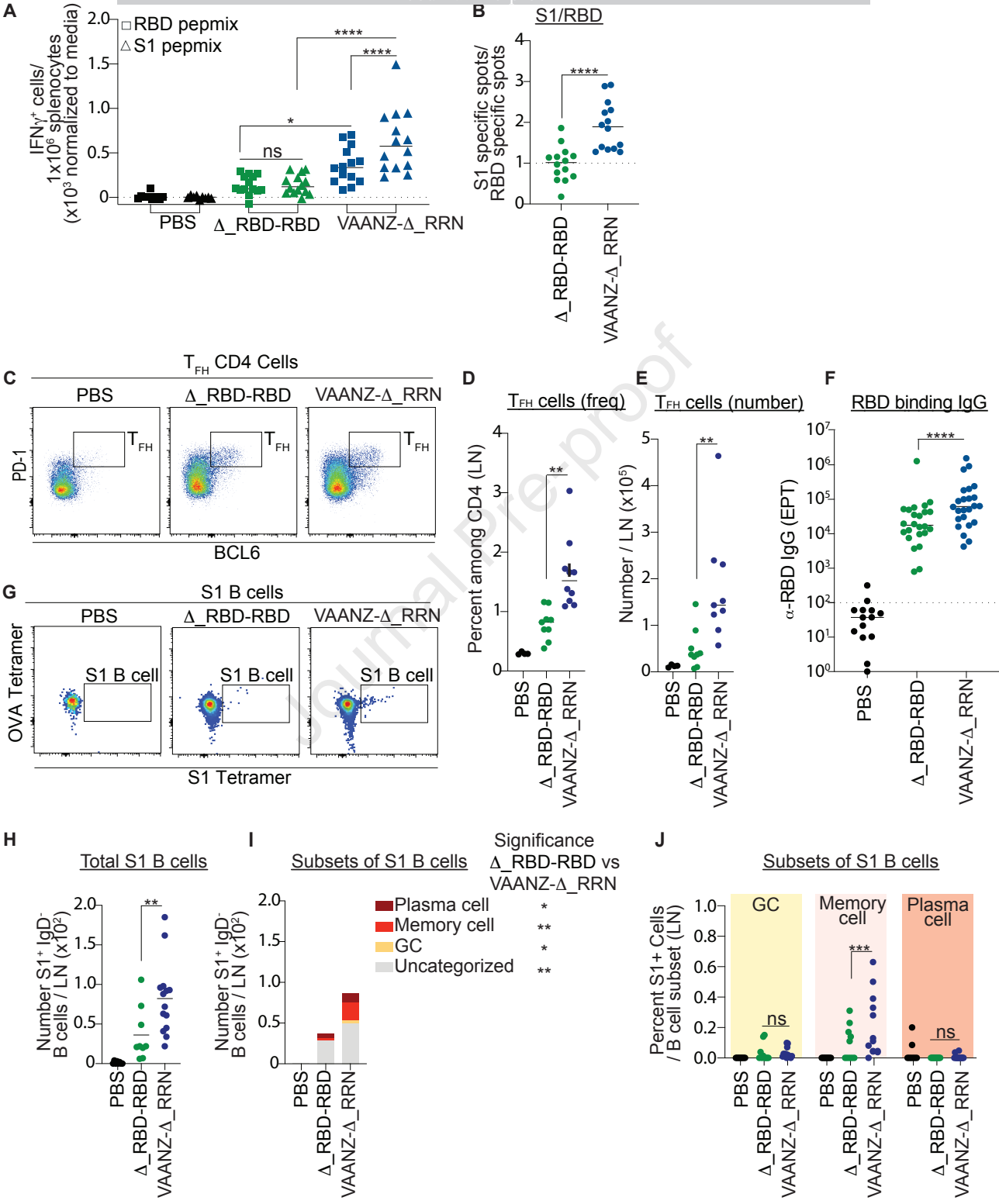

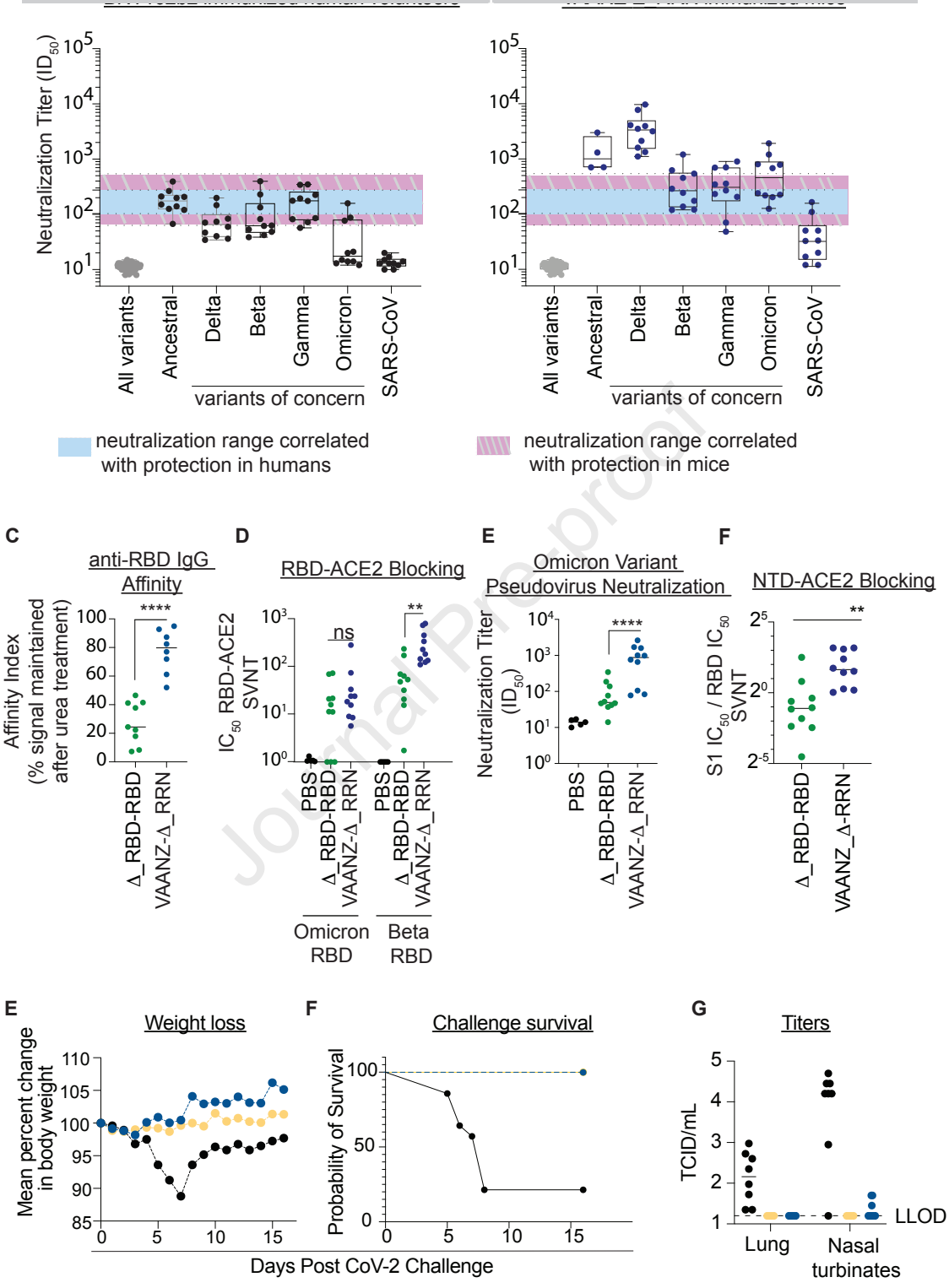

Highlights

- Novel vaccine construct, VAANZ-Δ_RRN, generates high protein yield.
- Immunization with VAANZ-Δ_RRN stimulates improved immunity compared to RBD dimer.
- VAANZ-Δ_RRN elicits abroad humoral responses, through high affinity RBD and NTD IgG.
- VAANZ-Δ_RRN immunization protects against live challenge with variants of concern.